Inorganic Chemistry

Article

pubs.acs.org/IC

A DFT-Elucidated Comparison of the Solution-Phase and SAM Electrochemical Properties of Short-Chain Mercaptoalkylferrocenes: Synthetic and Spectroscopic Aspects, and the Structure of Fc−CH_2CH_2−S−S−CH_2CH_2−Fc

Jan P. Lewtak,[†] Marilé Landman,[‡] Israel Fernández,[§] and Jannie C. Swarts*[,†]

[†]Department of Chemistry, University of the Free State, P.O. Box 339, Bloemfontein 9300, Republic of South Africa

[‡]Department of Chemistry, University of Pretoria, Private Bag X20, Hatfield 0028, Republic of South Africa

[§]Departamento de Química Orgánica I, Facultad de Ciencias Químicas, Universidad Complutense de Madrid, 28040 Madrid, Spain

Supporting Information

ABSTRACT: Facile synthetic procedures to synthesize a series of difficult-to-obtain mercaptoalkylferrocenes, namely, $Fc(CH_2)_nSH$, where n = 1 (**1**), 2 (**2**), 3 (**3**), or 4 (**4**) and Fc = $Fe(\eta^5\text{-}C_5H_5)(\eta^5\text{-}C_5H_4)$, are reported. Dimerization of **1**−**4** to the corresponding disulfides **19**−**22** was observed in air. Dimer **20** (Z = 2) crystallized in the triclinic space group $P\bar{1}$. Dimers **20**−**22** could be reduced back to the original $Fc(CH_2)_nSH$ derivatives with $LiAlH_4$ in refluxing tetrahydrofuran. Density functional theory (DFT) calculations showed that the highest occupied molecular orbital of **1**−**4** lies exclusively on the ferrocenyl group implying that the electrochemical oxidation observed at ca. $-15 < E_{pa} < 76$ mV versus FcH/FcH^+ involves exclusively an Fe(II) to Fe(III) process. Further DFT calculations showed this one-electron oxidation is followed by proton loss on the thiol group to generate a radical, $Fc(CH_2)_nS^{\bullet}$, with spin density mainly located on the sulfur. Rapid exothermic dimerization leads to the observed dimers, $Fc(CH_2)_n$−S−S−$(CH_2)_n$Fc. Reduction of the ferrocenium groups on the dimer occurs at potentials that still showed the ferrocenyl group $\Delta E = E_{pa,monomer} - E_{pc,dimer} \leq 78$ mV, indicating that the redox properties of the ferrocenyl group on the mercaptans are very similar to those of the dimer. ^{1}H NMR measurements showed that, like ferrocenyl oxidation, the resonance position of the sulfhydryl proton, SH, and others, are dependent on $-(CH_2)_n-$ chain length. Self-assembled monolayers (SAMs) on gold were generated to investigate the electrochemical behavior of **1**−**4** in the absence of diffusion. Under these conditions, ΔE approached 0 mV for the longer chain derivatives at slow scan rates. The surface-bound ferrocenyl group of the metal-thioether, $Fc(CH_2)_n$ −S−Au, is oxidized at approximately equal potentials as the equivalent CH_2Cl_2-dissolved ferrocenyl species **1**−**4**. Surface coverage by the SAMs is dependent on alkyl chain length with the largest coverage obtained for **4**, while the rate of heterogeneous electron transfer between SAM substrate and electrode was the fastest for the shortest chain derivative, Fc-CH_2−S−Au.

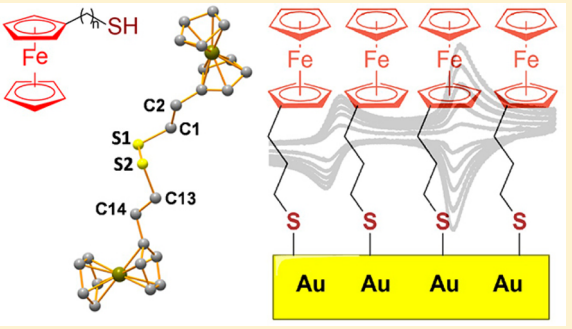

INTRODUCTION

Ferrocene derivatives have been well-studied over the last few decades because of their broad spectrum of applications[1] in fields as diverse as catalysis,[2] cancer therapy,[3] in energy transfer processes,[4] and also as molecular sensors[5] or as components in light-emitting diodes.[6] The ease by which ferrocene can be functionalized[7] led to a systematic investigation of substituent effects on the reversible redox properties[8] of the electron-donating[9] ferrocenyl group. Small changes in substituent can fine-tune the redox behavior of the ferrocenyl group with profound effects on the catalytic[10] and anti-neoplastic activity of the complexes.[3,11] Thus, it was shown that electron-rich ferrocene-containing rhodium complexes undergo faster oxidative addition[10] (the rate-determining step in the Monsanto process of converting methanol to acetic acid)[12] than electron-poor rhodium complexes, while studies on a series of ferrocene-containing acids[11] and alcohols[3a] of the type $Fc(CH_2)_nCOOH$ and $Fc(CH_2)_mOH$ (n = 0−3, m = 1−4, and Fc = $Fe^{II}(\eta^5\text{-}C_5H_5)(\eta^5\text{-}C_5H_4)$) indicated that the lower the redox potential of the ferrocenyl group is, the more cytotoxic it becomes.

Thiols, also known as mercaptans or sulfhydryls, are compounds bearing a −SH functionality. Simple organic thiols are known for their odors[13] and are used to treat acute toxicosis in cattle.[14] Disulfides are formed by coupling of two thiol groups under mild oxidative conditions. Such disulfide bridges are frequently found in proteins, where they determine protein stability and folding.[15] Thiol interactions with metals lead to complexes having the metal-thioether (M−S−R) bonding

Received: December 18, 2015

DOI: 10.1021/acs.inorgchem.5b02936
Inorg. Chem. XXXX, XXX, XXX−XXX

Scheme 1. Synthesis[a] of Mercaptoalkylferrocenes 1−4

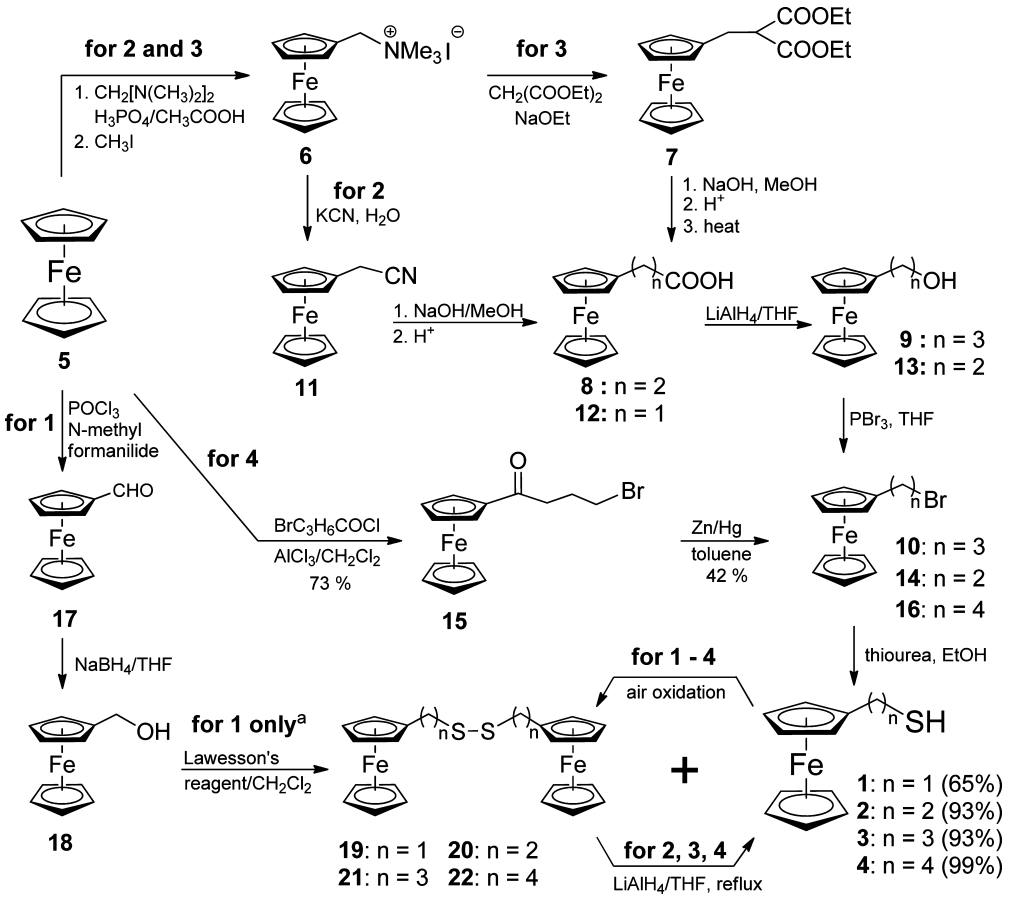

[a]Lawesson's reagent gives mixtures of **19** and **1** in ratios up to 1:2.2. The dimers **20**, **21**, and **22** cannot be obtained from suitable alcohols utilizing Lawesson's reagent. They form spontaneously by air oxidation of **2**, **3**, and **4**. Dimer **19** cannot be reduced to **1** with $LiAlH_4$.

motif; some of them have practical applications. For example, bismuth-thiolates exhibit a broad spectrum antimicrobial activity useful for protection of water supplies, and they are capable of inhibiting biofilm formation.[16] The interaction of thiols as well as disulfides with gold leads to self-assembled monolayers (SAMs) on gold surfaces[17] via Au−S−R bond formation. Although general synthetic routes to thiols are available,[18] information on the synthesis of simple short-chain mecaptoalkylferrocenes is lacking. Razumas[19] and colleagues investigated the hybrid compound series $FcCX(CH_2)_nCOO(CH_2)_9SH$ (X = O or H_2; n = 2, 3) possessing an ester functional group within the mercapto-alkyl side chain. In these complexes, the SH and Fc functionalities are separated by 14 or 15 atoms. Two reports[20,21] have been published where the synthesis of true, long alkyl chain ($n \geq 4$) mercaptoferrocenes, $Fc(CH_2)_nSH$, are described. However, spectroscopic characterization of the compounds was lacking. Moreover, the reported pathway for mercaptoalkylferrocene synthesis (ferrocene → ferrocenoylalkyl bromide → bromoalkylferrocene → mercaptoalkylferrocene) can only be applied to ferrocene-containing mercaptans with alkyl chain length of four carbons or longer. The synthesis of derivatives with shorter chains (n = 1, 2, or 3) with this synthetic protocol fails during the reduction of the ferrocenoylalkyl bromide because of the labilizing effect the electron-rich ferrocenyl moiety has on the terminal bromide.

Although reduction of ferrocenoylalkyl bromide may sometimes be achieved if very mild reducing agents such as sodium cyanoborohydride are used, in this work we describe optimized, reproducible, multistep synthetic routes to obtain $Fc(CH_2)_nSH$ with n = 1, 2, 3, and 4 from the corresponding alcohol, report the spectroscopic behavior of these complexes as well as of the oxidized dimers $Fc(CH_2)_n-S-S-(CH_2)_nFc$, and compare the electrochemical properties of $Fc(CH_2)_nSH$ in CH_2Cl_2 solutions with those of $Fc(CH_2)_n-S-Au$ SAMs on a gold electrode. In addition, the single-crystal structure of $Fc(CH_2)_2-S-S-(CH_2)_2Fc$ is presented, and density functional theory (DFT) calculations are used to gain more insight into the electrochemistry of the novel compounds.

RESULTS AND DISCUSSION

Synthesis. The syntheses of **1**−**4** are highlighted in Scheme 1. The synthetic approach reported for long-alkyl chain ferrocenyl sulfides ($n \geq 4$) by Creager[20] was used to obtain **4**, which possesses a four-carbon alkyl chain. This method involved first Friedel−Crafts acylation of ferrocene **5** with 4-bromobutyryl chloride to give solid 4-bromo-1-butyrylferrocene, **15**, in 73% yield. Acylation time to obtain **15** was optimized and found to be 20 h (Supporting Information, Figure S1). The keto functionality of **15** was then reduced by Clemmensen reduction[22] to give 4-bromobutylferrocene, **16**, in 42% as an orange oil. Refluxing of **16** in ethanol in the presence of thiourea followed by refluxing in aqueous NaOH liberated almost quantitatively 4-mercaptobutylferrocene, **4**. The overall yield of **4** from ferrocene was ca. 30%. Complex **4** was

DOI: 10.1021/acs.inorgchem.5b02936
Inorg. Chem. XXXX, XXX, XXX−XXX

previously synthesized by Cattabriga[23] and also Creager[24] to study SAMs on mercury, gold, and silver.

The same approach to obtain bromides **10** and **14**, the precursors to **2** and **3** (acylation of ferrocene and reduction of the product), failed. Ferrocene acylation with 3-bromopropionyl chloride[25] resulted in 3-bromopropionylferrocene as one of the components in the crude mixture of two products that were inseparable using chromatographic methods. The crude mixture was then subjected to Clemmensen reduction, but no bromide **10** was detected among the products. As for **14**, bromoacetylferrocene could be isolated, but the ensuing Clemmensen reduction resulted in in situ debromination; ethylferrocene rather than the expected 2-bromoethylferrocene, **14**, was isolated. This contrasts with Marrani's results,[26] who, unfortunately, did not supply analytical or synthetic details of their compounds. Different solvents (toluene, trichlorobenzene) and reaction times also failed to liberate the required bromoalkylferrocenes **10** and **14**.

From our failed attempts to obtain **10** and **14** utilizing the Creager[24] approach, we conclude that short-chain ketoalkyl bromide precursors, such as $FcCO(CH_2)_2Br$, are significantly less stable than their longer chain ($n \geq 4$) counterparts and that Clemmensen reduction is not suitable for carbonyl reduction of ferrocenoylbromoalkanes if the carbon side chain length possesses three carbon atoms or less. Other reducing methods are known,[22,27] but we searched here for an alternative synthetic protocol to obtain the desired ferrocenoylbromoalkanes **10** and **14**. This required the synthesis of ferrocenylalcohols **9**, **13**, and **18** (Scheme 1).[28]

Alcohol **9**, $Fc(CH_2)_3OH$, was obtained in a multistep synthesis that included a nucleophilic substitution reaction between **6** and diethylmalonate in the presence of a base, followed by hydrolysis and decarboxylation. Subsequent reduction of 3-ferrocenylpropanoic acid, **8**, with $LiAlH_4$ gave 3-hydroxypropylferrocene, **9**, in near quantitative yield. 2-Hydroxyethylferrocene, **13**, was obtained (Scheme 1) by treating **6** first with KCN to produce nitrile **11**, followed by basic hydrolysis to liberate ferrocenyl acetic acid **12** in 30% overall yield from ferrocene. $LiAlH_4$ reduction of acid **12** liberated 2-hydroxyethylferrocene **13** in quantitative yields. Because of the presence of the electron-rich ferrocene moiety, which highly affects stability of carbocations in close proximity to the ferrocenyl group, conversion of alcohols **9** and **13** to bromine derivatives **10** and **14** was achieved in 45% and 60% yield, respectively, provided special care was given to the dryness and purity of solvents and brominating agent PBr_3. Bromides **10** and **14** were treated in the same way as described above for **16** with thiourea to liberate 3-mercaptopropylferrocene, **3**, and 2-mercaptoethylferrocene, **2**, in good yields (Scheme 1). Complex **2** was previously patented[29] as nonmigrating burning rate modifier for unsaturated rubber-based propellants and was obtained by reacting vinyl ferrocene with thioacetic acid followed by hydrolysis of the thioester to liberate the thiol. Complex **3**, which was previously obtained using $NaBH_3CN$ as reductant and whose structure was solved,[30] was also studied on Au(111) layers by scanning tunnelling microscopy (STM) and to obtain field-emission resonances.[30]

Because of the strong electron-donating properties of the ferrocenyl moiety, the carbon adjacent to the cyclopentadienyl ring in ferrocenylmethanol **18** is unusually electron-rich. It is therefore prone to generate the carbocation $FcCH_2^+$, which possesses high stability[31] precluding the conversion of **18** into bromomethylferrocene. Bromomethylferrocene is, to the best of our knowledge, not described in the literature, probably due to the instability of this species as a result of the ease of $FcCH_2^+$ formation upon Br cleavage. Interestingly, 1,1′-dibromomethyleneferrocene is readily available.[32] Therefore, alcohol **18** was converted directly to sulfhydryl **1** using Lawesson's reagent (2,4-bis(4-methoxyphenyl)-1,3,2,4-dithiadiphosphetane-2,4-disulfide).[33] Lawesson's reagent is not appropriate to convert ethyl and longer-chain alcohols directly to thiols, but if a methanolic moiety is directly linked to an aromatic moiety, here ferrocenyl, thionation of an OH functionality with Lawesson's reagent offers good thiol yields.[34] Earlier literature reports on the synthesis of mercaptomethylferrocene[35] offer either very low yields or are irreproducible. In our hands, the synthesis of **1** utilizing Lawesson's reagent gave the desired thiol **1** together with disulfide **19** in ratios up to 2.2:1 (ca. 65% in the crude) after optimization of the reaction conditions (solvent, ratio of the substrates, temperature, time of the reaction). Separation of **1** and **19** using standard column chromatography methods were very inefficient due to the rapid dimerization of mercaptomethylferrocene **1**. Pure **1** was eventually isolated in 45% yield using preparative thin-layer chromatography (TLC) while maintaining strictly inert conditions.

After thiols **2**−**4** were stored for up to three weeks in air, substantial although undesired disulfide formation (compounds **20**−**22**, Scheme 1) was observed; mercaptomethylferrocene, **1**, is fully converted to disulfide **19** in a matter of hours in air. The rate of dimerization is a function of alkyl chain length—increasing resistance to air-induced thiol oxidation is observed for higher "*n*" values. In solution, air oxidation of thiols **1**−**4** to disulfides occurs faster than in the solid state. The disulfides have much higher melting points than the thiols, probably because intermolecular secondary and tertiary van der Waals forces are more accessible in disulfides than in thiols. For example, disulfide **20** melts at 101 °C compared to the 44 °C melting point of thiol **2**. It is possible to reduce disulfides **20**−**22** back to mercaptans **2**−**4** with $LiAlH_4$ in boiling tetrahydrofuran (THF, Scheme 1) but not with $NaBH_4$. All attempts to reduce $FcCH_2-S-S-CH_2Fc$, **19**, to $FcCH_2SH$, **1**, met with no success.

Structure of 20. Determination of the single-crystal X-ray structures of **19**−**22** was complicated due to a tendency to form multiple domain crystals (**19**, **20**) or solvation to form amorphous oils (**21**, **22**) upon crystallization. However, crystallographic quality crystals of **20** could be obtained from hexane; it crystallizes in the triclinic space group $P\bar{1}$. Refinement parameters and crystal data are summarized in the Experimental Section. The molecular structure of **20** highlighting atom labeling is shown in Figure 1. Selected bond distances and bond angles are summarized in the caption of Figure 1, but the full set of bond lengths and angles is available in Supporting Information.

In terms of the ferrocenyl groups of **20**, the average C−C bond distance within the ferrocenyl groups is 1.389 Å for the unsubstituted cyclopentadienyl rings and 1.413 Å for substituted cyclopentadienyl rings. The largest deviations from this average are +0.151 Å for C(20)−C(24) and −0.086 Å for bond C(21)−C(22). Angles C(21)−C(22)−C(23) and C(24)−C(20)−C(21) of the unsubstituted cyclopentadienyl ring coordinated to Fe(2) deviated the most from the ideal average of 108° in both unsubstituted and the substituted cyclopentadienyl rings, +3.1° and −4.7°, respectively. Each of the separate ferrocenyl groups thus exhibits the

DOI: 10.1021/acs.inorgchem.5b02936
Inorg. Chem. XXXX, XXX, XXX−XXX

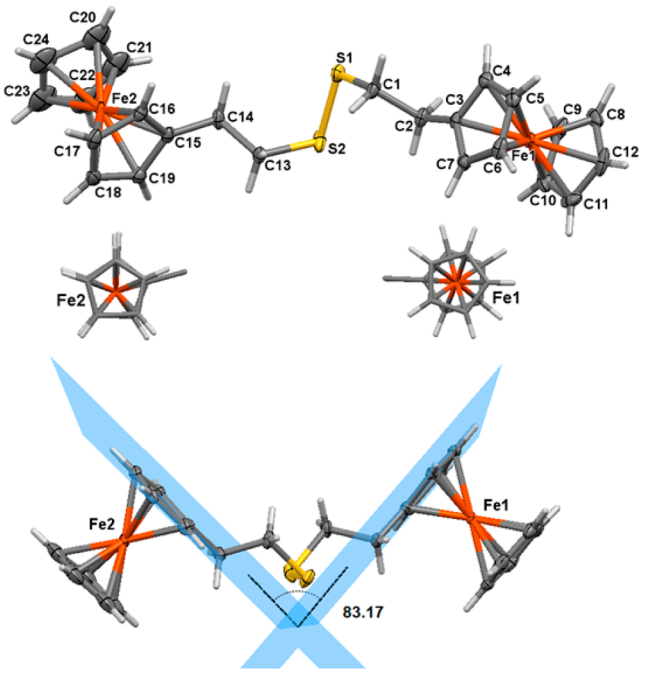

Figure 1. (top) Molecular structure of $Fc(CH_2)_2–S–S–(CH_2)_2Fc$, **20**, highlighting atom labeling. Thermal ellipsoids are drawn at 50% probability level. Selected bond distances (Å) and angles (deg) are S(1)–S(2) 2.025(5), S(1)–C(1) 1.800(6), S(2)–C(13) 1.805(6), C(1)–C(2) 1.513(6), C(13)–C(14) 1.508(6), C(2)–C(3) 1.490(6), C(14)–C(15) 1.490(7), $C–C_{average}$ (substituted Cp ring) 1.413 (7), $C–C_{average}$ (unsubstituted Cp ring) 1.389(10), $Fe(1)–C(x)_{average}$ (x = 3–7) 2.031(6), $Fe(1)–C(x)_{average}$ (x = 8–12) 2.032(6), $Fe(2)–C(x)_{average}$ (x = 15–19) 2.025(7), $Fe(1)–C(x)_{average}$ (x = 20–24) 2.017(8), C(1)–S(1)–S(2) 103.6(2), C(13)–S(2)–S(1) 103.6(2), S(1)–C(1)–C(2) 112.4(3), C(1)–C(2)–C(3) 111.6(4), C(2)–C(3)–C(4) 124.8(4), C(4)–C(3)–C(7) 108.3(4), C(3)–C(4)–C(5) 107.7(4), C(4)–C(5)–C(6) 108.4(4), C(5)–C(6)–C(7) 107.7(4), C(6)–C(7)–C(3) 107.9(4). Torsion angles (cent = centroid): C(1)–S(1)–S(2)–C(13) 90.2, C(3)-cent(subst-Cp-ring)-cent(Cp-ring)-C(10) −33.7 staggered, C(15)-cent(subst-Cp-ring)-cent(Cp-ring)-C(21) 7.0, eclipsed. (insets) The staggered and eclipsed conformations of ferrocenyl fragments Fe1 and Fe2 are highlighted. (bottom) Nearly perpendicular planes between the two ferrocenyl substituents. Symmetry transformations used to generate equivalent atoms, No. 1 $-x, -y, -z$.

expected normal delocalized bond lengths and angles. The average Fe–C bond lengths for ferrocenyl substituent Fc1 containing Fe(1) and Fc2 containing Fe(2) are 2.028 Å for the substituted and 2.025 Å for the unsubstituted rings. Ferrocenyl fragment Fc1 lies parallel with the S(2)–C(13) bond, while Fc2 lies parallel with the S(1)–C(1) bond. They also lie nearly perpendicular to one another as is evidenced by the angle of 83.2° between the two planes defined by the substituted ring of each ferrocenyl substituent (Figure 1). However, the two ferrocenyl groups were found to differ in conformation. Ferrocenyl substituent Fc1 exhibited a staggered cyclopentadienyl ring conformation (deviation from eclipse = 33.7°), while the other approached the eclipsed form (deviation from eclipse = 7.0°).

The S(1)–S(2) bond length of 2.025(5) Å for **20** compares well with those found in literature. For example, the S–S bond length of the related literature complex, (2*RS*,5*SR*)-2,5-diferrocenyl-1,6-dibenzoyl-3,4-dithiahexane, **A**, is 2.019 Å.[36] This value appears to be representative for complexes containing a $–CH_2–CHR–S–S–CHR–CH_2–$ chain fragment in its structure.[37−40] By contrast, the S(1)–C(1) and S(2)–C(13) bond distances of **20** are on average 0.01–0.03 Å shorter than in these cited complexes. The C(1)–S(1)–S(2)–C(13) dihedral angle of **20**, 90.2°, also compares well with the average of those of the cited literature complex (86.7°).

^{1}H NMR Spectroscopy. The lack of proper spectroscopic data of mercaptoalkylferrocenes in literature can be understood because the ^{1}H NMR spectra of thiols **1**–**4** are difficult to record in well-readable form. To prevent air oxidation yielding disulfides, measurements must be made under a strictly inert atmosphere.

The sulfhydryl proton (S<u>H</u>) of **1**, **3**, and **4** is observable as triplets due to coupling with neighboring methylene protons. For **2**, we were unable to record a spectrum that successfully resolved the resonances of the SH protons from a multiplet into a triplet. Upon elongation of the alkyl chains of **1**–**4**, the chemical shift of SH resonance moves toward higher fields (smaller δ values). This is a consequence of the diminished deshielding effect of the ferrocenyl moiety that distorts the magnetic field around SH in moving from alkyl chain lengths of n = 1 to n = 4. Other long-chain alkyl-substituted aromatic compounds such as phthalocyaninyl-,[41] phthalonitrilylalkyls,[41] and ferrocenylalkylalcohols[28] show a similar deshielding effect on the resonance position of the phthalocyanylic, benzylic, ferrocyclic, and neighboring CH_2 protons. Figure 2 shows the

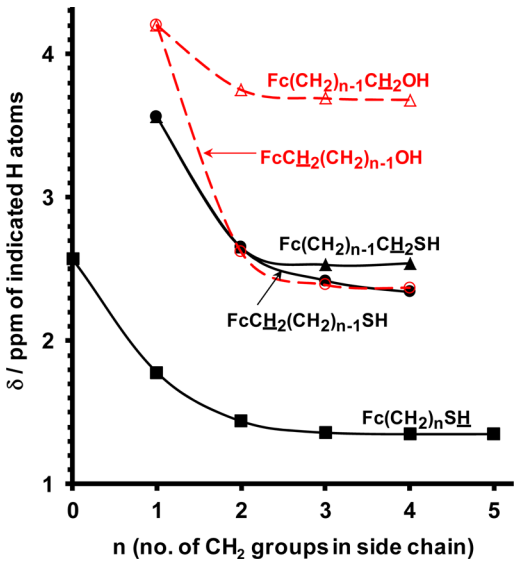

Figure 2. Relationship between the ^{1}H NMR position (δ values/ppm) of the indicated protons and the number of CH_2 spacers n separating the ferrocenyl group from an OH or SH functionality in $Fc(CH_2)_nOH$ (red lines)[28] and $Fc(CH_2)_nSH$ (black lines; data for compounds with n = 0[42] and n = 5[20] were taken from literature).

dependence of the position of the underlined proton resonances S<u>H</u>, $Fc(CH_2)_{n-1}C\underline{H}_2SH$, $FcC\underline{H}_2(CH_2)_{n-1}SH$ and also for the resonances of the indicated ferrocenylalcohol CH_2 groups in $Fc(CH_2)_{n-1}C\underline{H}_2OH$, $FcC\underline{H}_2(CH_2)_{n-1}OH$ on the alkyl side chain connecting the ferrocenyl group with the OH or SH functionality.

Although the electron-donating properties of the ferrocenyl group may also play a role in the observed ^{1}H NMR peak position shift, it is considered a minor influence because compounds exhibiting stronger electron-donating effects on a

DOI: 10.1021/acs.inorgchem.5b02936
Inorg. Chem. XXXX, XXX, XXX–XXX

particular proton grouping are expected to shift peak positions of that proton grouping upfield (to smaller δ values), not downfield. The SH functional group of the short chain compounds **1** and **2** would be expected to experience the electron-donating power of the ferrocenyl group the strongest, while the longer chain derivatives would experience it the weakest. If the electron-donating power of the ferrocenyl group was the strongest factor to influence the chemical shifts, the resonating position of SH group of the shortest chain derivatives **1** and **2** should be at the smallest δ-value (biggest upfield shift), and **4** would exhibit the SH resonance at the largest δ-value (smallest upfield shift). Figure 2 shows this clearly not to be the case. Interestingly, the resonance positions of the ferrocyl CH_2 protons of $FcC\underline{H}_2(CH_2)_{n-1}SH$ and $FcC\underline{H}_2(CH_2)_{n-1}OH$ asymptotically strive to the same δ-value at $n = 4$ (Figure 2) despite the big difference in these resonance positions for compounds with $n = 1$. In contrast, the resonances of the CH_2 protons neighboring the SH group in **4**, $Fc(CH_2)_3C\underline{H}_2SH$, are found at δ = 2.54 ppm, while for $FcCH_2)_3C\underline{H}_2OH$ they are found at δ = 3.68 ppm. This is in accordance with the stronger electron-withdrawing properties of an oxygen atom (Pauling scale electronegativity = 3.4) over that of a sulfur atom (electronegativity = 2.6).

The ^{1}H NMR spectrum of **20** showed a much more complicated coupling pattern compared to thiol **2**. The shape of signals indicates an AA′BB′ pattern, where each A proton couples differently to the B and B′ protons. This effect is often seen when the chemical shift difference of protons A and B (ν_{AB}) approaches the value of J_{AB} coupling. Resonance shape complexity is determined by the difference in relative sizes of J_{AB} and $J_{AB'}$, which has its source in conformational properties of R′−CH_2CH_2−R″ fragments. This implies that there must be a preference for one over the other conformation (*anti*/*gauche*). An experiment in which spectra of **20** were recorded at different temperatures shows that the population of the *anti* and *gauche* conformations of CH_2−CH_2 fragments strives to a statistical ratio of 1:2, and this portion of the spectrum mimics an A_2B_2 pattern, Figure 3. Furthermore, at higher temperatures

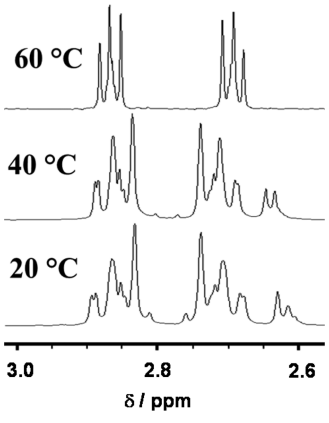

Figure 3. Variable-temperature ^{1}H NMR ($CDCl_3$, 300 MHz) showing the CH_2 resonances of disulfide 20, $Fc(CH_2)_2$−S−S−$(CH_2)_2$Fc.

(60 °C), the resonance pattern of the CH_2−CH_2 fragment of **20** simplified into the normal, expected triplets. Therefore, at this temperature, no preferred *anti* or *gauche* conformations can be detected. A wide ^{1}H NMR spectrum of **1**, **2**, **3**, **4**, and **20** may be found in Supporting Information, Figures S2−S6.

Electrochemical and Density Functional Theory Studies. Cyclic voltammetry (CV) of mercaptoalkylferrocenes **1**−**4** were conducted in CH_2Cl_2 containing 0.2 M $[N(^nBu)_4][PF_6]$ as supporting electrolyte under argon utilizing a glassy carbon working electrode for solution studies and a gold electrode for SAM electrochemistry. The solution CV studies highlighted analyte electrochemical behavior subject to diffusion effects, while SAM coatings of thiols **1**−**4** on a gold electrode surface allowed demonstration of their electrochemical behavior in the absence of diffusion effects. Cyclic voltammograms are shown in Figures 4 and 6, while Table 1 contains a summary of electrochemical data. Potentials are reported versus the FcH/FcH^+ couple, but experimentally they were recorded with decamethylferrocene, Fc*, as internal standard.

The redox behavior of **1**−**4** in solution at slow scan rates (100 mV s^{-1}) approached electrochemical reversibility, since ΔE values were between 60 and 78 mV, Table 1. Theoretically, electrochemical reversible solution-phase redox processes are characterized by $\Delta E = E_{pa} - E_{pc}$ = 59 mV and i_{pc}/i_{pa} ratios of 1.[43,44] Only **4** exhibited an i_{pc}/i_{pa} ratio close to one (0.98). Compounds **1**−**3** exhibited $0.77 \leq i_{pc}/i_{pa} \leq 0.80$.

The inset in Figure 4, left, highlights the linear dependence of peak currents against the square root of scan rate for solution-based cyclic voltammograms according to the Randles−Sevcik[43] equation, eq 1.

$$i_p = 0.4463nFAC(nF\upsilon D/RT)^{0.5} \quad (1)$$

Utilizing this equation and the data of Figure 4, after determination of the accurate surface area of the glassy carbon electrode by CV techniques according to published procedures[45] as 3.0988 mm^2, apparent diffusion constant of **4** under our experimental conditions was calculated to be $D = 1.56 \times 10^{-9}$ m^2 s^{-1}. The other complexes have apparent diffusion constants close to this value, Table 1.

To gain more insight into the observed electrochemical parameters (Table 1), DFT calculations were performed, first to confirm that it is really the Fc group of **1**−**4** that is oxidized in the electrochemical experiment and not the SH group. Figure 5 highlights that, for **1** and **4**, the highest occupied molecular orbitals (HOMOs) lie exclusively on the iron atom, implying the observed oxidation involves the generation of Fe(III) exclusively. Indeed, the computed spin densities on the corresponding $[Fc\text{-}(CH_2)_n\text{-}SH]^{\bullet+}$ species indicate a value of ca. 1.2 e on the iron atom of $\mathbf{1}^{\bullet+}$ as well as $\mathbf{4}^{\bullet+}$. These results therefore support that the oxidation process involves exclusively the Fe(II) to Fe(III) transformation. It can be suggested that, under air conditions, a proton is then lost to generate the $Fc\text{-}(CH_2)_n\text{-}S^{\bullet}$ radical. Interestingly, the computed spin density on the $Fc\text{-}(CH_2)\text{-}S^{\bullet}$ species is mainly located at the sulfur (0.84 e) with only a small contribution at the iron atom (0.13 e), which suggests an intramolecular electron transfer from the iron to the sulfur atom upon deprotonation. Finally, a highly exothermic dimerization (ΔE = −52.9 kcal/mol) of this radical occurs then to produce the experimentally observed dimer. During all this time, the ferrocenyl groups are continuously being oxidized to the ferrocenium cation radical. On the reverse sweep, the ferroceniums on the dimer are reduced back to ferrocenyl groups.

Figure 6, left, compares the CVs of **1**−**4** with each other. Clearly, the formal reduction potential, $E^{o\prime} = (E_{pa} + E_{pc})/2$, decreases systematically but nonlinearly with increase in alkyl

DOI: 10.1021/acs.inorgchem.5b02936
Inorg. Chem. XXXX, XXX, XXX−XXX

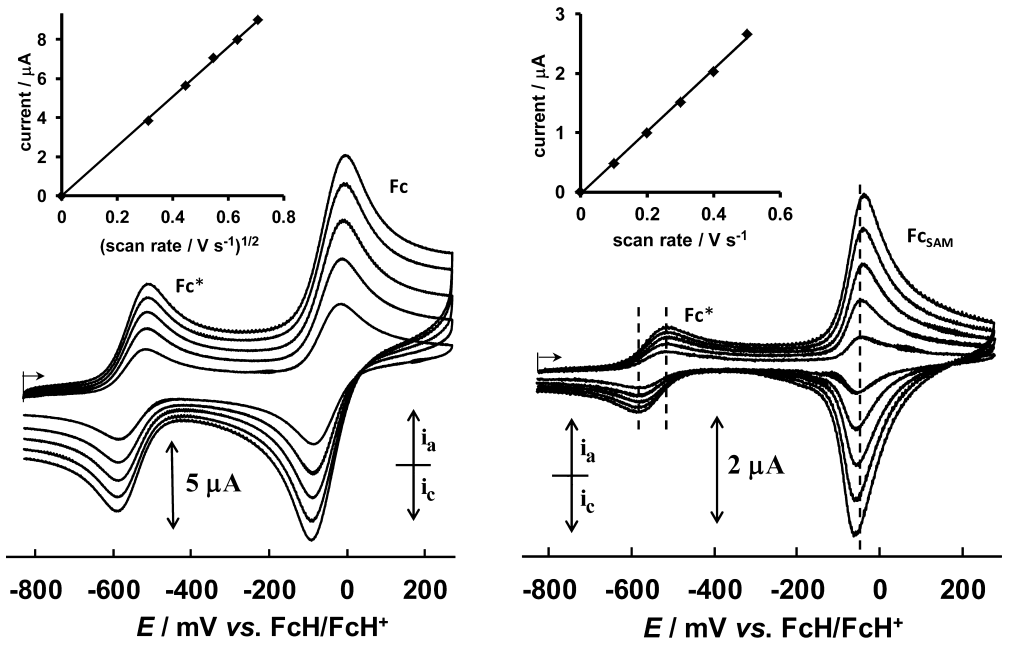

Figure 4. Cyclic voltammograms of **4** in CH_2Cl_2 containing 0.2 mol dm^{-3} $[N(^nBu)_4][PF_6]$ at a scan rates at 100, 200, 300, 400, and 500 mV s^{-1} (left) in solution phase (analyte concentration is 0.5 mmol dm^{-3}; Fc indicates the ferrocenyl wave of **4**) and (right) as self-assembled monolayers on a gold electrode. Fc_{SAM} indicates the ferrocenyl wave of **4** when bound to the Au electrode with A_{sur} = 1.972 mm^2 after a roughness correction was performed; the surface concentration was found to be 2.74 × 10^{-10} mol cm^2. (insets) The linear relationship between anodic current and either the square root of scan rate in solution cyclic voltammogram or scan rate itself when **4** is surface-bound as a SAM layer. Fc* = decamethylferrocene, the *dissolved* internal standard in both experiments.

Table 1. Cyclic Voltammetry Data[a] of ca. 0.25 mmol dm^{-3} Solutions of 1−4 in CH_2Cl_2 Containing 0.2 mol dm^{-3} $[N(^nBu)_4][PF_6]$ at a Scan Rate 100 mV s^{-1}

	E_{pa}, mV	ΔE_p, mV	$E^{o\prime}$, mV	i_{pa}, μA	i_{pc}/i_{pa}	1 × 10^9 D[b]	$PW_{0.5}$[c]	1 × 10^{10} Γ[d]	k_s, s^{-1} [e]
1 (n = 1)	71; (85)	78; (116)	32; (27)	1.68; (0.84)	0.77; (0.89)	1.24; (−)	184; (288)	- ; (0.86)	- ; (3.9)
2 (n = 2)	14; (36)	60; (32)	−16; (20)	1.70; (1.91)	0.78; (0.95)	1.27; (−)	172; (144)	- ; (1.93)	- ; (3.8)
3 (n = 3)	−4; (16)	74; (22)	−41; (5)	1.84; (2.16)	0.80; (0.98)	1.48; (−)	224; (196)	- ; (2.23)	- ; (3.2)
4 (n = 4)[f]	−14; (-50)	74; (11)	−50; (-55)	3.78; (2.66)	0.95; (0.99)	1.56; (−)	184; (110)	- ; (2.74)	- ; (5.2)

[a]All potentials are reported vs the FcH/FcH^+ couple at 0.0 V. The values in parentheses are for **1**−**4** as SAMs on a gold electrode in the same solvent and supporting electrolyte but in the absence of any free analyte at a scan rate of 500 mV s^{-1}. [b]Estimations of diffusion constants (a solution-phase result only) in units of m^2 s^{-1} utilizing the Randles−Sevcik equation, eq 1. [c]$PW_{0.5}$ = "full width at half of the peak maximum height" in units of mV at a scan rate of 100 mV s^{-1}; ideal reversibility for SAM's require $PW_{0.5}$ to be 90.6 mV. The solution-phase $PW_{0.5}$ values are given for comparison with SAM values only, but it has no physical meaning as solution-phase CV waves do not have Gaussian shapes. [d]Γ = SAM surface concentration in units of mol cm^{-2}. A roughness correction was performed; see text. [e]k_s = measured heterogeneous electron transfer rates between ferrocenyl group and electrode under the experimental conditions employed. Because of uncertainties, especially for the decay current of each compound (**1** is most inaccurate), these values serve to give trends, but are estimates only. [f]Concentration of **4** is not 0.25 but 0.5 mM.

chain length. Figure 7 highlights this relationship and compares it with the relationship obtained for an equivalent series of compounds, Fc-$(CH_2)_n$−OH.[28] Redox potentials strove to an asymptotic minimum at $n \approx 4$ in a manner similar to what was found in the ^1H NMR spectra, Figure 2. Figure 5 also explains why the redox potential for the ferrocenyl alcohols is smaller than those of the corresponding short-chain mercaptans. The calculated energy of the HOMO of Fc-CH_2−OH, the orbital from which the electron is released, is −5.24 − (−5.39) = +0.15 eV less stabilized than in Fc-CH_2−SH. Therefore, an electron is much easier released during oxidation of Fc-CH_2−OH than during oxidation of the mercaptan, Fc-CH_2−SH, which is reflected in the smaller redox potentials for the alcohols shown in Figure 7.

Electrochemistry of Self-Assembled Monolayers. Mercaptans can be immobilized on a gold surface. Complexes **1**−**4** were anchored via metal-thioether (Au−S−R) bonds on the surface of a gold electrochemistry electrode, Scheme 2, by dipping the gold electrode in a 0.25 mmol dm^{-3} solution of analyte in CH_2Cl_2 containing 0.2 mol dm^{-3} $[NBu_4][PF_6]$ for 1 h followed by thorough rinsing with CH_2Cl_2. Longer dipping times (2 or 4 h) did not result in significant changes in the coverages reported in Table 1. This enabled us to study the electrochemistry of the surface-bound metal-thioethers in the absence of diffusion effects and also without the complication of dimerization, as metal-thioethers do not dimerize. As commented earlier, the STM study of **3** on a Au(111) surface as well as the field-emission resonances of **3** supported on a gold surface by STM were reported previously.[30] In addition, SAMs of complex **4** were previously studied on mercury,[23] gold, and silver surfaces.[24]

For complete electrochemical reversible systems, anodic and cathodic waves of SAM systems should be symmetrical, and $\Delta E = E_{pa} - E_{pc}$ should be 0 mV.[46] The relationship between peak currents and scan rate is given by eq 2,[46] where A_{sur} is the electrode surface area, and Γ is the surface coverage.

DOI: 10.1021/acs.inorgchem.5b02936
Inorg. Chem. XXXX, XXX, XXX−XXX

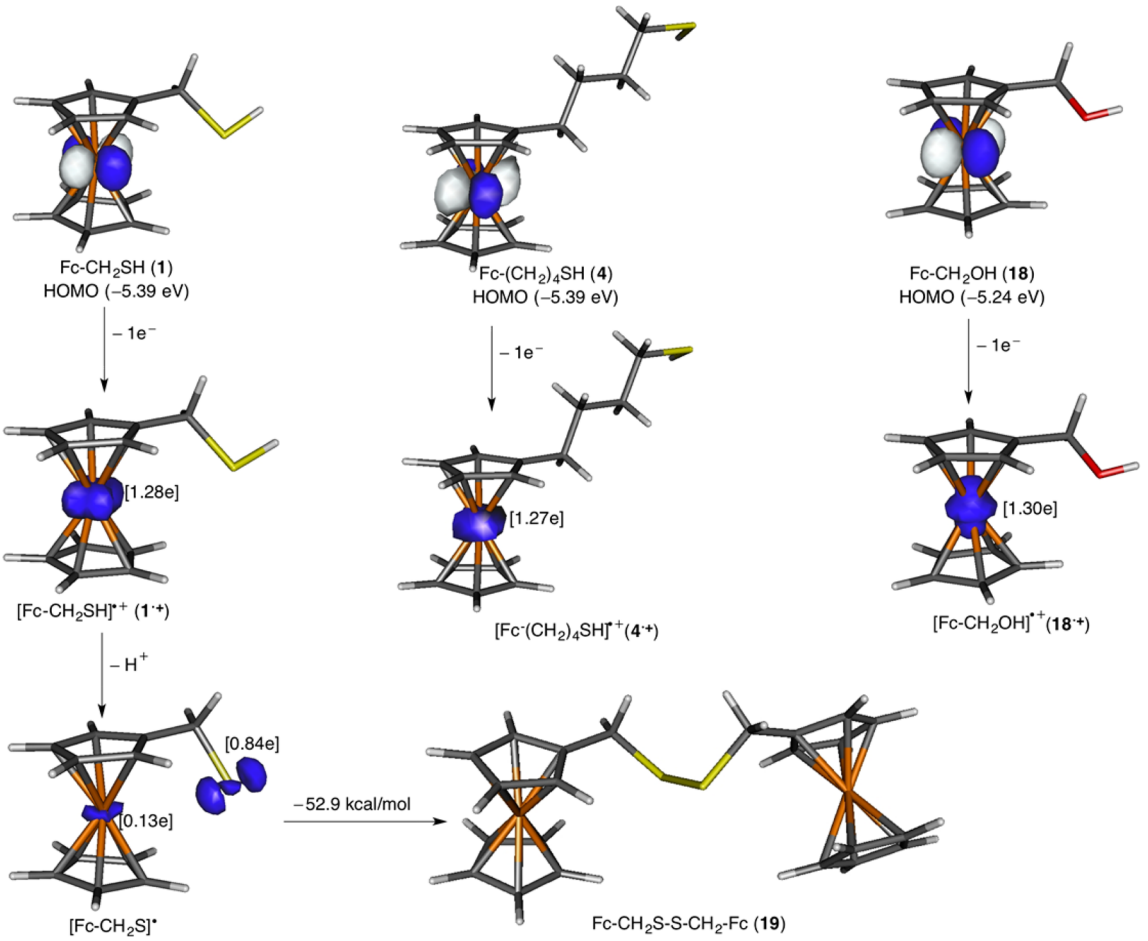

Figure 5. Computed HOMOs of complexes **1** (top left), **4** (middle top), and $FcCH_2OH$ (top right) and spin densities of the corresponding oxidized species (middle and bottom). Numbers in parentheses indicate the computed Mulliken-spin densities. All data were computed at the B3LYP/def2-SVP level.

$$i_p = (n^2F^2\upsilon A_{sur}\Gamma)/(4RT) \quad (2)$$

To use eq 2 meaningfully, the term A_{sur} needs to be corrected from the suppliers geometric electrode surface area value (here the supplied geometrical data of the gold electrode indicated a diameter of 1.6 mm, which leads to a theoretical A_{sur} of 2.010 619 mm^2) to a roughness corrected experimental surface area. The experimental surface area can be determined from CV measurements utilizing the Randles–Sevcik equation applied to ferrocene under known conditions.[45] This allows for a "roughness" correction of the electrode that takes into account the rugosity of the gold electrode under the conditions utilized. Under previously described CV conditions[45] we determined A_{sur} of our gold electrode as 1.972 mm^2, which implies a roughness correction of 0.981. This correction factor was employed in all appropriate calculations shown in Table 1.

From eq 2, for surface bound species, a linear relationship should exist between i_p and scan rate υ. The coverage Γ is also available from the slope of this graph. In addition, peak shape is diagnostic of the homogeneity of the layer and the "full width at half of the peak maximum height", $PW_{0.5}$, should theoretically be 90.6 mV at 25 °C for one-electron transfer processes.[46]

Figure 4 right shows the CV traces of a SAM of **4** on a gold electrode in the presence of dissolved decamethylferrocene as internal standard. The nearly symmetric shape of the cyclic voltammograms are apparent: ΔE = 11 mV, and the anodic $PW_{0.5}$ = 116 mV at a scan rate of 500 mV s^{-1}. This implies that, for **4** with n = 4, nearly ideal electrochemistry of the SAM is observed. Figure 6, right, shows the cyclic voltammograms at 500 mV s^{-1} for SAM layers of **1**–**4**. From it, and from the data summarized in Table 1, it is clear that the electrochemical behavior becomes less and less ideal as the alkyl chain length (i.e., "n" in $Fc(CH_2)_nSH$) decreases. First, in moving from **4** to **3**, ΔE increases to 22 mV. For **1**, ΔE = 116 mV is so large it casts doubt as to whether SAM formation actually took place. However, from the cleaning procedures used to clean the SAM-containing gold electrode from any free **1**, and because the relationship between i_{pa} and υ is still linear (Supporting Information Figure S7), while the relationship between i_{pa} and $\upsilon^{0.5}$ is not (Supporting Information Figure S8), it becomes evident that **1** is a surface-associated species on Au, although the integrity of the layer under electrochemically oxidative conditions may not be as good as that of **2**–**4**. The low electrode coverage obtained for **1** (see below) may contribute to the large ΔE observed in CV experiments of SAM layers of this compound. In an attempt to increase the coverage, exposure times of 16 h during SAM preparations of this complex were also employed, but it did not improve the coverage obtained.

Values of full width at half peak maximum height, $PW_{0.5}$, were determined at a scan rate of 100 mV s^{-1}, Table 1. Those for **2** (144 mV) and **4** (110 mV) approached the ideal value of 90.6 mV best, while **1** deviated the most. Deviations from the

DOI: 10.1021/acs.inorgchem.5b02936
Inorg. Chem. XXXX, XXX, XXX–XXX

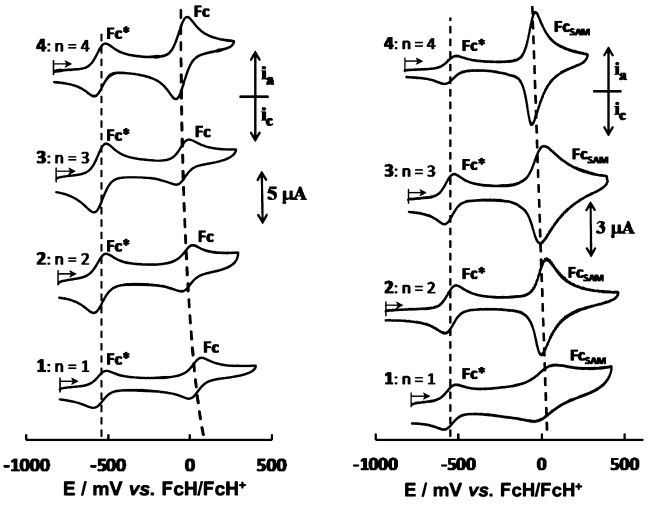

Figure 6. CVs of **1**−**4**, $Fc(CH_2)_nSH$, from (left) 0.25 or 0.5 mmol dm^{-3} (for **4**) solutions in CH_2Cl_2 containing 0.2 mol dm^{-3} $[N(^nBu)_4][PF_6]$ supporting electrolyte at a scan rate 100 mV s^{-1} utilizing a glassy carbon electrode or (right) as self-assembled monolayers on a gold electrode at a scan rate of 500 mV s^1. Fc indicates the ferrocenyl wave in the solution experiments, and Fc_{SAM} identifies the ferrocenyl wave of **1**−**4** when bound to the Au electrode in electrode surface concentrations as per Table 1. Fc* indicates the CV wave of decamethylferrocene, the *dissolved* internal standard in both experiments.

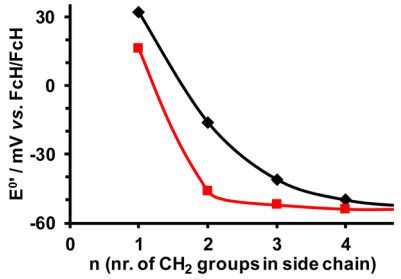

Figure 7. Relation between $E^{o\prime}$ and the number of CH_2 spacers n separating the ferrocenyl group from the SH functionality in $Fc(CH_2)_nSH$ in compounds **1**−**4** (black line) or from OH in $Fc(CH_2)_nOH$ (red line).[28]

Scheme 2. Formation of SAMs of 1−4 on a Gold Electrode

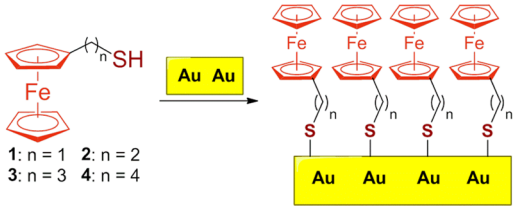

ideal value are attributed to electrostatic effects incurred by neighboring charged species, here the $Fc^{\bullet+}$ radical cation, or with supporting electrolyte anions after electrochemical oxidation of neutral **1**−**4** occurred.[47]

Surface coverages Γ were determined from the slopes of plots of i_{pa} versus scan rate utilizing eq 2 and are summarized in Table 1. Obtained values compared well with the maximum expected surface coverage of 4.4×10^{-10} mol cm^{-2} for a ferrocenyl fragment having the normally accepted diameter of 0.66 nm and being closely packed in a hexagonal assembly on a flat (here gold) surface.[19] The obtained coverage values are a function of side chain length. The longest side chain in **1**−**4** has $n = 4$. The coverage obtained for **1** having $n = 1$ was only 31% of that obtained for **4**.

The heterogeneous rate of electron transfer between ferrocenyl group and electrode, k_s, under the utilized experimental conditions, may be calculated from eq 3.

$$k_s = i_p/Q \tag{3}$$

The amount of charge, Q, may be obtained from the area of CV waves in Figure 6, right, with the baseline drawn to exclude background currents.[46] The x-axis of the diagram has to be modified not to be potential but seconds, utilizing the scan rate employed (see Experimental Section and Supporting Information Figures S9−S16). Only anodic waves were considered. The obtained values of k_s are summarized in Table 1. The k_s values do not show a direct relationship with n or $E^{o\prime}$. The rate constant k_s for **1** was the second largest; we were surprised to note our measurements indicate that the rate of heterogeneous electron transfer for **4** is the largest, but for **1** it is the second fastest. On the basis of side chain length, one would expect this rate for **4** to be the smallest. Figure 8 shows how coverage and heterogeneous electron transfer kinetics under our conditions are dependent on side chain length, and it also shows how redox potentials influence k_s.

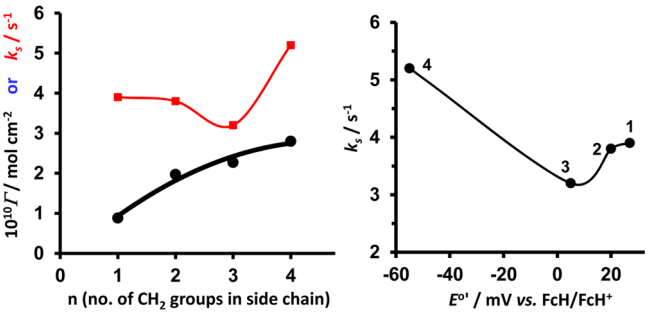

Figure 8. (left) Dependence of electrode surface coverage, Γ (thick black line) and rate of heterogeneous electron transfer between electrode surface and redox-active ferrocenyl groups, k_s (red line), on the alkyl side chain length n of SAM layers of Fc-$(CH_2)n$-SH on a gold electrode. (right) Dependence of k_s on $E^{o\prime}$ of **1**−**4** when bound as SAM layers on a gold electrode. Compound numbers are indicated on the graph.

Two opposing electron transfer driving forces may be the reason for the faster-than-expected heterogeneous electron transfer kinetics of **4** and the shape of the n−k_s relationship shown in Figure 8. The first relates to the lower electrochemical energy required to induce electron transfer in compounds with smaller redox potentials compared to those with larger redox potentials. Because $E^{o\prime}$ values of the SAMs of **1**−**4** are the largest for **1** and the smallest for **4**, it would be reasonable to expect (provided all other factors remain the same) that the rate of electron transfer for **4** should be the fastest, while it should be the slowest for **1**. However, directly opposing this, one could also expect that the close proximity of the ferrocenyl group of the shortest chain derivative, **1**, to the electrode surface would greatly favor faster electron transfer for **1** over that of **4**. These two opposing driving forces may be at the root of explaining the trend that the rate constant data in Figure 8 and Table 1 exhibits.

Finally, an attempt was made to measure the inherent rate of electron transfer (i.e., k_{ET}) from the ferrocenyl group of **1**−**4** to

DOI: 10.1021/acs.inorgchem.5b02936
Inorg. Chem. XXXX, XXX, XXX−XXX

a gold electrode when the complexes are bound to the surface of the electrode via a Au−S−CH $_2$− metal-thioether bond utilizing the Laviron method.[46,48] However, this met with failure as we could not scan fast enough (υ_{max} was 2500 V s^{-1}) to reach the region where ΔE_p values became large enough and $E_p - E_{1/2}$ became linearly dependent on log(scan rate), Figure S17. The expected scan rate to achieve this would be in excess of 100 000 V s^{-1} which, because of large currents and therefore large ohmic loss, probably takes this experiment outside the realms of CV. However, utilizing published data for k_{ET} for complexes with $5 \leq n \leq 12$,[46] a calibration curve of n versus log(k_{ET}), Figure S18, resulted in the following, more acceptable values: (n; k_{ET}/s^{-1}) = (1; 2×10^9), (2; 5×10^8), (3; 2×10^8), and (4; 5×10^7). Other reports also described a linear relationship between n versus log(k_{ET}) for ferrocenylamido-thiolates[49] for compounds having 7−17 methylene groups between S and ferrocenylamido groups and also other substrates such as hydroquinone-terminated thiols.[50] In the latter cases, because of much slower electron transfer rates, data are available all the way down until one methylene spacer between S and the redox-active terminal. Of the so-obtained k_{ET} values, the values for complexes with n = 3 and 4 are probably more accurate as the described calibration curve does not account for different electrostatic, steric, and other effects that may become important with exceedingly short side chain lengths.

CONCLUSIONS

The mercaptoalkylferrocenes $Fc(CH_2)_nSH$ series with n = 1 (**1**), 2 (**2**), 3 (**3**), and 4 (**4**) was synthesized. They are all prone to easy sulfhydryl oxidation, and the corresponding disulfides **19**−**22** form spontaneously in air. Except for the short-chain dimer **19**, these disulfides can all be reduced back to the original mercaptoalkylferrocenes in refluxing THF with $LiAlH_4$. Key precursors to **1**−**4** were the ferrocenylalkyl bromides $Fc(CH_2)_nBr$. The instability of these bromides with $n < 4$ forced their synthesis from alcohol precursors rather than Clemmensen reduction of $FcCO(CH_2)_{n-1}Br$. Only conversion of the shortest chain alcohol **1** having n = 1 can be achieved by Lawesson's reagent. ^{1}H NMR resonance positions of all CH_2 and SH functionalities were dependent on alkyl side chain length n. The electrochemical mechanism of $Fc(CH_2)_nSH$ oxidation in solution was explored by DFT methods, and it was found that solely the ferrocenyl group is oxidized during the initial solution-based oxidation. Then, after proton loss and intramolecular electron transfer, a radical species $Fc(CH_2)_nS^{\bullet}$ is obtained, which very quickly dimerizes in a strongly exothermic process. The cathodic wave during the solution-based electrochemical process therefore represents the reduction of the ferroceniums on the dimer. A similar complication was not observed during electrochemical studies of SAMs of **1**−**4** on a gold electrode, as the $Au-S(CH_2)_nFc$ metallothioether species is not prone to dimerization. Here, only a ferrocenyl/ferrocenium redox couple is observed. It also highlighted fast ferrocenyl group electron transfer in the absence of diffusion effects. ΔE_p values approached zero for the surface-bound mercaptans, because the substrate was immobilized on the electrode surface, while diffusion effects caused ΔE values for the solution-based species to be ca. 75 mV. Formal redox potentials $E^{o\prime}$ of **1**−**4**, both in solution and as self-assembled monolayers on a gold electrode, are dependent on alkyl side chain length n. The extent of gold electrode coverage by $Fc(CH_2)_nSH$ is also dependent on chain length with the shortest chain derivative being the least effective in SAM formation. This is probably the result of steric hindrance of the bulky ferrocenyl group impairing effective coverage. The heterogeneous rate of electron transfer between the ferrocenyl group of each SAM could not directly be measured, as they are too fast, but it is estimated to be in the region from 1×10^7 to 1×10^9 s^{-1}.

EXPERIMENTAL SECTION

General. All chemicals (Aldrich) were used as received unless otherwise stated. Solvents (hexane, THF, diethyl ether) were distilled over sodium wire prior to use. CH_2Cl_2 was distilled over $CaCl_2$. Chromatography was performed on silica gel 60 (220−240 mesh, Fluka); reaction progress was monitored using silica-coated TLC plates. NMR spectra were recorded on a Bruker Avance 300 spectrometer. Chemical shifts are reported in δ values, using deuterated solvent residual peak as internal standard. IR spectra (cm^{-1}) were recorded on a Bruker Tensor 27 spectrometer with a PIKE MIRacle ATR-attachment. Compounds **6**,[51] **7**,[52] **8**,[53] **9**,[52] **11**,[54] **12**,[53] **13**,[55] **14**,[53] **15**,[56] **17**,[57] and **18**[58] were synthesized according to the literature procedures.

Synthesis. *Mercaptomethylferrocene (**1**).* To a solution of ferrocenylmethanol **18** (216 mg, 1 mmol) in dry CH_2Cl_2 (10 mL), Lawesson's reagent (201 mg, 0.5 mmol) was added. The reaction was stirred at room temperature under an inert atmosphere for 1 h. NMR analysis showed the reaction solution containing crude product consisted of a mixture of **1** and dimer **19**, Fc−CH_2−S−S−CH_2−Fc, with ratio of **1**:**19** = 2.2:1. Evaporation of solvent gave a residue that was suspended in Et_2O and loaded onto preparative TLC under argon. Utilizing the deaerated solvent mixture hexane/EtOAc = 9:1 as eluent, the first fraction gave mercaptomethylferrocene **1** as a deep orange oil (104 mg, 45%). The second fraction gave **19** as an orange solid (100 mg, 44%).

*Characterization Data for Mercaptomethylferrocene (**1**).* R_f = 98:2 (hexane/ethyl acetate) = 0.50; orange oil. Anal. Calcd for $C_{11}H_{12}FeS$, C, 56.9; H, 5.2%. Found: C, 56.6; H, 5.0%. ^{1}H NMR (300 MHz, $CDCl_3$, ppm) δ 1.78 (t, 1H, J = 7.4 Hz, SH) 3.56 (d, 2H, J = 7.4 Hz, CH_2), 4.15 (t, 1.8 Hz, CH_2), 4.18 (s, 5H, Cp), 4.23 (t, 1.8 Hz, 2H, Cp); ^{13}C NMR (75 MHz, $CDCl_3$, ppm) 24.4, 67.9 (2C), 68.0 (2C), 68.7 (5C), 88.4; IR (neat, υ_{max}/cm^{-1}): 3628, 2960, 2522, 2444, 2159, 2030, 1976, 1249, 1101, 1026, 998, 806, 668.

*Characterization Data for Bis(ferrocenylmethyl)disulfide (**19**).* mp 129 °C; R_f = 0.40 (hexane/ethyl acetate = 98:2). Anal. Calcd for $C_{22}H_{22}Fe_2S_2$, C, 57.2; H, 4.8%. Found: C, 57.4; H, 4.9%. ^{1}H NMR (300 MHz, $CDCl_3$, ppm) δ 3.49 (s, 4H, CH_2), 4.13−4.15 (m, 14 H, Cp), 4.20 (t, 1.8 Hz, 4H, Cp); ^{13}C NMR (75 MHz, $CDCl_3$, ppm) 31.9 (2C), 67.9 (4C), 68.0 (4C), 68.7 (10C), 85.3 (2C); IR (neat, υ_{max}/cm^{-1}): 3076, 2943, 2911, 1468, 1409, 1243, 1216, 1103, 999, 827, 715, 601.

Synthesis of Mercaptoalkylferrocenes 2, 3, and 4. First bromoalkylferrocenes and precursors must be synthesized.

*4-Bromobutanoylferrocene (**15**).* Bromobutyryl chloride (236 mg, 1.5 mmol) and anhydrous $AlCl_3$ (200 mg, 1.5 mmol) were added to 4 mL of dry CH_2Cl_2 at 0 °C. The mixture was stirred for 20 min under argon and then added dropwise to a solution of ferrocene (279 mg, 1.5 mmol) in CH_2Cl_2 (4 mL). After 20 h the reaction was quenched with water (2 mL). The organic layer was washed with water until it was neutral. Evaporation of solvent afforded a brown residue that was chromatographed (SiO_2, hexane/EtOAc = 4:1) to give **15** in 73% of yield. mp 62 °C; R_f (hexane) = 0.40; ^{1}H NMR (300 MHz, $CDCl_3$, ppm) δ 2.29 (quin, 2H, J = 6.6 Hz, CH_2CH_2), 2.96 (t, 2H, J = 6.6 Hz, CH_2Br), 3.59 (t, 2H, J = 6.6 Hz, CH_2CO), 4.23 (s, 5H), 4.54 (t, 2H), 4.83 (t, 2H); ^{13}C NMR (75 MHz, $CDCl_3$, ppm) 27.50, 34.6, 38.0, 69.7 (2C), 70.2 (2C), 73.6 (5C), 73.2, 201.2; IR (neat, υ_{max}/cm^{-1}) 2998, 2926, 1666, 1452, 1409, 1302, 1033, 750.

Synthesis of Bromoalkylferrocenes 10, 14, and 16. *3-Bromopropylferrocene (**10**).* The synthesis of **10** may serve as general example. 3-Hydroxypropylferrocene (**9**, 0.650 g, 2.67 mmol) was dissolved in dry Et_2O (5 mL), and freshly distilled PBr_3 (91 μL,

DOI: 10.1021/acs.inorgchem.5b02936
Inorg. Chem. XXXX, XXX, XXX−XXX

2.9 mmol) was added under an inert atmosphere. The reaction mixture was stirred for 3 h. Column chromatography with SiO_2 using hexane/EtOAc = 2:1 as eluent afforded 370 mg (45%) of pure **10**. mp 49 °C; R_f = 0.55 (hexane); ^{1}H NMR (300 MHz, $CDCl_3$, ppm) δ 2.07 (q, 2H, J = 7.6 Hz, CH_2CH_2), 2.53 (t, 2H, J = 7.6 Hz, CH_2CH_2) 3.44 (t, 2H, J = 7.6 Hz, CH_2CH_2), 4.08−4.10 (m, 4H), 4.14 (s, 5H); ^{13}C NMR (75 MHz, $CDCl_3$, ppm) 28.00, 33.7, 33.9, 67.4 (2C), 68.2 (2C), 68.6 (5C), 87.2; IR (neat, υ_{max}/cm^{-1}) 3089, 3076, 2924, 2895, 2871, 2841, 1455, 1434, 1281, 1043, 999, 805.

Characterization Data for 14 and 16. *2-Bromoethylferrocene (**14**).* Yield = 60%; mp 66 °C; R_f = 0.60 (hexane); ^{1}H NMR (300 MHz, $CDCl_3$, ppm) δ 2.93 (t, 2H, J = 7.6 Hz, CH_2CH_2), 3.47 (t, 2H, J = 7.6 Hz, CH_2CH_2), 4.08−4.18 (m, 9H); ^{13}C NMR (75 MHz, $CDCl_3$, ppm) 32.4, 33.7, 67.7 (2C), 68.3 (2C), 68.6 (5C), 85.5; IR (neat, υ_{max}/cm^{-1}): 3092, 2923, 2850, 1466, 1442, 1275, 1206, 1104, 1023, 807, 715, 616.

*4-Bromobutylferrocene (**16**).* Yield = 42%; R_f = 0.70 (hexane); orange oil; ^{1}H NMR (300 MHz, $CDCl_3$, ppm) δ 1.63−1.72 (m, 2H, CH_2), 1.78−1.88 (m, 2H, CH_2), 2.39 (t, J = 7.5 Hz, $FcCH_2$), 3.57 (t, J = 7.5 Hz, 2H, CH_2Br) 4.08 (s, 4H), 4.13 (s, 5H); ^{13}C NMR (75 MHz, $CDCl_3$, ppm) 28.8, 29.5, 32.5, 34.6, 67.3 (2C), 68.2 (2C), 68.6 (5C), 86.4; IR (neat, υ_{max}/cm^{-1}): 3093, 2935, 2857, 1441, 1292, 1227, 1105, 999, 816, 729, 647.

Synthesis of Mercaptoalkylferrocenes 2, 3, and 4. *2-Mercaptoethylferrocene (**2**).* The synthesis of **2** may serve as general example. 2-Bromoethylferrocene (**14**, 438 mg, 1.5 mmol) was dissolved in absolute ethanol (10 mL). Thiourea (84 mg, 1.1 mmol) was added, and the reaction was refluxed for 18 h. The solvent was evaporated, aqueous NaOH (2 M, 10 mL) was added, and it was heated under reflux for an additional hour under an inert atmosphere (argon). After it cooled, the mixture was extracted with Et_2O (3 × 50 mL), and the combined organic fractions were washed thoroughly with brine (1 × 100 mL). Evaporation of the solvent gave a yellow residue, which was chromatographed on silica with eluent hexane/EtOAc = 98:2, to afford 343 mg (93%) of pure **2**. R_f = 0.40 (hexane); mp = 44 °C. Anal. Calcd for $C_{12}H_{14}FeS$, C, 58.6; H, 5.7%. Found: C, 58.7; H, 5.7%. ^{1}H NMR (300 MHz, $CDCl_3$, ppm) δ 1.41−1.47 (m, 1H, SH), 2.63−2.67 (m, 4H, CH_2CH_2), 4.06−4.13 (m, 9H); ^{13}C NMR (75 MHz, $CDCl_3$, ppm) 25.8, 34.6, 67.5 (2C), 68.3 (2C), 68.6 (5C), 86.6. IR (neat, υ_{max}/cm^{-1}): 3083, 2924, 2853, 1466, 1439, 1238, 1104, 1023, 998, 807.

Characterization Data for 3 and 4. *3-Mercaptopropylferrocene (**3**).* Yield = 94%; R_f = 0.65 (hexane); mp = 34 °C. Anal. Calcd for $C_{13}H_{16}FeS$, C, 60.0; H, 6.2%. Found: C, 59.7; H, 6.1%. ^{1}H NMR (300 MHz, $CDCl_3$, ppm) δ 1.36 (t, J = 7.8 Hz, 1H, SH), 1.82 (tt, 2H, J_1 = J_2 = 7.8 Hz, CH_2), 2.45 (t, 2H, J = 7.8 Hz, $FcCH_2$), 2.55 (dt, J_1 = J_2 = 7.8 Hz, 2H, CH_2S), 4.06 (s, 4H), 4.11 (s, 5H); ^{13}C NMR (75 MHz, $CDCl_3$, ppm) 24.7, 28.5, 35.5, 66.2 (2C), 67.5 (2C), 68.8 (5C), 88.3. IR (neat, υ_{max}/cm^{-1}): 3087, 3077, 2930, 2841, 2561, 1435, 1297, 1102, 1044, 999, 804.

*4-Mercaptobutylferrocene (**4**).* Yield = 99%; R_f = 0.65 (hexane); mp = 27 °C. Anal. Calcd for $C_{14}H_{18}FeS$, C, 61.3; H, 6.6%. Found: C, 61.4; H, 6.5%. ^{1}H NMR (300 MHz, $CDCl_3$, ppm) δ 1.35 (t, J = 7.8 Hz, 1H, SH), 1.58−1.68 (m, 4H, CH_2CH_2), 2.34 (t, 2H, $FcCH_2$), 2.54 (dt, J_1 = J_2 = 7.8 Hz, 2H, CH_2S) 4.05 (s, 4H), 4.10 (s, 5H); ^{13}C NMR (75 MHz, $CDCl_3$, ppm) 24.8, 29.4, 30.1, 34.1, 67.4 (2C), 68.3 (2C), 68.8 (5C), 89.1. IR (neat, υ_{max}/cm^{-1}): 3090, 2920, 2849, 2344, 1458, 1410, 1039, 999, 815.

Disulfides 20−22. Exposure to air resulted in oxidation of **2**, **3**, and **4** to disulfides **20**, **21**, and **22**, respectively. The crude product was purified by column chromatography on silica gel utilizing hexane as eluent to afford pure disulfide. Characterization data are as follows:

*Bis(2-ferrocenylethyl)disulfide (**20**).* Yield is 35% after 7 d. R_f (hexane) = 0.36; mp = 100−101 °C. Anal. Calcd for $C_{24}H_{26}Fe_2S_2$, C, 58.8; H, 5.3%. Found: C, 58.7; H, 5.1%. ^{1}H NMR (300 MHz, $CDCl_3$, ppm) δ 2.77 (AA′ of AA′BB′, 4H, CH_2), 2.86 (BB′ of AA′BB′, 4H, CH_2), 4.08−4.12 (m, 8H, Cp), 4.13 (s, 10H, Cp); ^{13}C NMR (75 MHz, $CDCl_3$, ppm) 29.8 (2C), 39.7 (2C), 67.5 (4C), 68.2 (4C), 68.6 (10C), 86.8 (2C). IR(neat, υ_{max}/cm^{-1}): 3075, 2910, 2847, 1416, 1401, 1040, 1034, 1020, 806.

*Bis(3-ferrocenylpropyl)disulfide (**21**).* Yield is 20% after 7 d. R_f (hexane) = 0.40; mp = 80.7 °C. Anal. Calcd for $C_{26}H_{30}Fe_2S_2$, C, 60.2; H, 5.8%. Found: C, 60.4; H, 5.8%. ^{1}H NMR (300 MHz, $CDCl_3$, ppm) δ 1.93 (q, J = 7.5 Hz, 4H, CH_2), 2.47 (t, J = 7.5 Hz, 4H, $FcCH_2$), 2.73 (t, J = 7.5 Hz, 4H, CH_2S) 4.08−4.09 (m, 8H), 4.13 (s, 10H); ^{13}C NMR (75 MHz, $CDCl_3$, ppm) 28.2 (2C), 30.3 (2C), 38.5 (2C), 67.2 (4C), 68.1 (4C), 68.5 (10C), 88.1 (2C). IR (neat, υ_{max}/cm^{-1}): 3086, 2918, 2849, 1433, 1408, 1227, 1103, 999, 807.

*Bis(4-ferrocenylbutyl)disulfide (**22**).* Yield is 8% after 7 d. R_f (hexane) = 0.45; mp = 46.5 °C. Anal. Calcd for $C_{12}H_{14}FeS$, C, 61.6; H, 6.3%. Found: C, 61.3; H, 6.1%. ^{1}H NMR (300 MHz, $CDCl_3$, ppm) δ 1.59−1.66 (m, 4H, 2xCH_2), 1.67−1.77 (m, 4H, CH_2CH_2), 2.37 (t, J = 7.5 Hz, 4H, $FcCH_2$), 2.71 (t, J = 7.2 Hz, 4H, CH_2S), 4.05 (s, 8H), 4.10 (s, 10H); ^{13}C NMR (75 MHz, $CDCl_3$, ppm) 29.1 (2C), 29.7 (2C), 29.9 (2C), 39.0 (2C), 67.1 (4C), 68.1 (4C), 68.5 (10C), 88.8 (2C). IR (neat, υ_{max}/cm^{-1}): 3091, 2925, 2854, 1409, 1039, 1023, 997, 815.

Reduction of Disulfides 20, 21, and 22. The general procedure for **20** may serve as an example. $LiAlH_4$ (10 mg, 0.25 mmol) was added to the solution of **20** (49 mg, 0.1 mmol) in dry THF (5 mL, degassed). After 1 h of reflux the reaction was quenched with HCl aq (5 mL, 5%) and extracted with Et_2O (3 × 5 mL). Combined organic layers were washed with brine (1 × 5 mL) and dried over $MgSO_4$. Evaporation of all volatiles afforded crystalline yellow **2** (40 mg, 81%).

X-ray Crystal Structure Determination of 20. Data for complex **20** were collected at 150(2) K on a Bruker D8 Venture κ geometry diffractometer, with duo Iμs sources, a Photon 100 CMOS detector, and APEX II control software using Quazar multilayer optics, monochromated Mo Kα radiation (0.710 73 Å), and by means of a combination of ϕ and ω scans. Data reduction was performed using SAINT+, and the intensities were corrected for absorption using SADABS.[59] The structure was solved by intrinsic phasing using SHELXTS and refined by full-matrix least-squares using SHELXTL and SHELXL-2013.[60] In the structure refinement, all hydrogen atoms were added in calculated positions and treated as riding on the atom to which they are attached. All nonhydrogen atoms were refined with anisotropic displacement parameters; isotropic displacement parameters for hydrogen atoms were calculated as $X \times U_{eq}$ of the atom to which they are attached; X = 1.5 for the methylene hydrogens and 1.2 for all other hydrogens. An Ortep drawing[61] of the structure is included in Figure 1. Crystallographic data and refinement parameters of **20** (C_{24} H_{26} Fe_2 S_2, M_r = 490.27, triclinic, $P\bar{1}$) are crystal size, 0.628 × 0.319 × 0.122 mm^3; cell dimensions, a = 5.794(13), b = 12.06(3), c = 16.07(4) Å, α = 111.24(12), β = 92.08(9), γ = 93.43(11)°, V = 1043(5) Å^3; Z = 2; density (calculated) = 1.562 Mg/m^3; absorption coefficient, 1.599 mm^{-1}; F(000), 508; Θ range for data collection, 2.640 to 25.681°; index ranges, $-7 \le h \le 7$, $-14 \le k \le 14$, $-19 \le l \le 19$; reflections collected, 13 315; independent reflections, 3763 [R(int) = 0.0441]; completeness to Θ = 25.242°, 99.9%; refinement method, full-matrix least-squares on F^2; final R indices [$I > 2\sigma(I)$], $R1$ = 0.0553, $wR2$ = 0.1464; R indices (all data), $R1$ = 0.0588, $wR2$ = 0.1497; largest difference peak and hole, 2.873 and −1.197 e·Å^{-3}; symmetry transformations used to generate equivalent atoms, No. 1 $-x$, $-y$, $-z$. Data collection, structure solution, and refinement details are available in the cif.

Computational Details. Geometry optimizations without symmetry constraints were performed using the Gaussian09 suite of programs[62] at the B3LYP level (uB3LYP for open-shell species)[63] using the double-ζ plus polarization def2-SVP[64] basis set for all atoms. This protocol is denoted B3LYP/def2-SVP and was selected because it provides reasonable results for rationalizing the electrochemical properties of different transition metal complexes, particularly those having ferrocenyl groups.[65] Zero-point vibrational energy corrections were computed at the same level and were not corrected. All species were characterized by frequency calculations[66] and have a positive defined Hessian matrix indicating that they are minima on the potential energy surface.

Electrochemistry. *Solution Cyclic Voltammetry.* Cyclic voltammograms were recorded on a Princeton Applied Research PARSTAT 2273 voltammograph utilizing PowerSuite (version 2.58) software.

DOI: 10.1021/acs.inorgchem.5b02936
Inorg. Chem. XXXX, XXX, XXX−XXX

Experiments were performed on ca. 0.25 mM solutions of **1**−**4** in dry CH_2Cl_2/0.2 mol dm^{-3} $[N(^nBu)_4][PF_6]$, utilizing a standard three-electrode cell consisting of a glassy carbon electrode of surface area 3.14 mm^2, a Pt-wire counter electrode, and an Ag-wire reference electrode under argon at 25 °C. The working electrode was pretreated by polishing on a Buehler micro cloth first with 1 μm and then with 1/4 μm diamond paste. Each experiment was first performed in the absence and then repeated in the presence of decamethylferrocene (Fc*). In separate experiments, a cyclic voltammogram of decamethylferrocene was measured in the presence of free ferrocene, and then all measured potentials were manipulated on a spreadsheet to allow reporting of potentials versus the FcH/FcH^+ couple at 0 V and diagram preparation. Under our conditions the Fc^*/Fc^{*+} redox couple was at $E^{o\prime}$ = −550 mV versus FcH/FcH^+, i_{pc}/i_{pa} = 0.99, and ΔE = 72 mV.[67]

Self-Assembled Monolayers Cyclic Voltammetry. After the solution-phase cyclic voltammograms were recorded, the glassy carbon electrode was replaced with a polished Au electrode (geometrical surface area according to the manufacturer is 2.010 619 mm^2, but the measured reactive surface area was found to be 1.972 mm^2; this leads to a roughness correction of 0.981) and allowed to stand for 1 h. The coated electrode having a monolayer of mercaptoalkylferrocene on it (SAM) was then removed, thoroughly rinsed with CH_2Cl_2 to remove all residues of the original solution, carefully dried with soft moisture-absorbing cloth, and then placed in a fresh solution containing 0.2 mol dm^{-3} $[N(^nBu)_4][PF_6]$ supporting electrolyte only. Cyclic voltammograms were then again recorded using a Ag wire pseudo reference electrode and a Pt-wire counter electrode. Experiments were conducted first in the absence and then in the presence of Fc* as internal standard. Data were then exported to a spreadsheet program for reporting purposes as described in Solution Cyclic Voltammetry.

Calculation of diffusion constants, surface coverage, and heterogeneous electron transfer rate constants (k_s) were performed with the aid of eqs 1, 2, and 3. To determine k_s, the amount of charge Q that flowed during a CV experiment may be obtained from the area underneath the CV waves in Figure 6, right, with the baseline drawn to exclude background currents.[46] The x-axis of the diagram must be modified not to be potential but seconds, utilizing the scan rate employed. Only anodic waves were considered. The nonideal shape of especially CVs of **1** and **3** caused us not to estimate the area of the "most appropriate surface" by measuring the area under the entire CV curve, because the decay current is obviously more affected by charge effects than the area under the rising current until E_p is reached. The area of that portion of the CV up to the peak anodic potential was measured and then multiplied with two to obtain the total "expected" or "more ideal" area. To measure the area, the CV data points were imported into Mettler Toledo thermal analysis STAR^e software. An appropriate baseline was determined, and then the area was calculated within appropriate boundaries; see Supporting Information Figures S9−S16.

Determination of k_{ET} was first attempted utilizing the method of Laviron[48] as described in Meade's review[46] (see Figure S17) but then alternatively estimated utilizing a calibration curve (Figure S18) as described elsewhere.[49,50]

■ ASSOCIATED CONTENT

Supporting Information

The Supporting Information is available free of charge on the ACS Publications website at DOI: 10.1021/acs.inorgchem.5b02936.

Optimisation results, spectroscopic data of ferrocene-containing mercaptans, electrochemical current-scan rate and -time relationships, a Laviron plot relating $E - E_{1/2}$ to log(scan rate), a calibration curve relating k_{ET} with alkyl chain length, and Cartesian coordinates and energies of all the species discussed in the text. (PDF)

X-ray crystallographic information. (CIF)

■ AUTHOR INFORMATION

Corresponding Author

*E-mail: swartsjc@ufs.ac.za.

Notes

The authors declare no competing financial interest.

■ ACKNOWLEDGMENTS

J.C.S. and J.P.L. acknowledge the NRF under Grant No. 2054243 and the UFS for financial support. I.F. acknowledges the Spanish MINECO-FEDER under Grant Nos. CTQ2013-44303-P and CTQ2014-51912-REDC. M.L. acknowledges the UP for financial support.

■ REFERENCES

(1) (a) *Ferrocenes;* Togni, A.; Hayashi, T., Eds.; VCH: Weinheim, Germany, 1995. (b) Deeming, A. J. In *Comprehensive Organometallic Chemistry;* Wilkinson, G., Stone, F. G. A., Abel, E. W., Eds.; Pergamon Press: Oxford, U.K, 1982; Vol. *8*, pp 475−491.

(2) (a) Shen, Q.; Shekhar, S.; Stambuli, J. P.; Hartwig, J. F. *Angew. Chem., Int. Ed.* **2005**, *44*, 1371. (b) Percec, V.; Bae, L.−Y.; Hill, D. H. *J. Org. Chem.* **1995**, *60*, 1060. (c) Swarts, P. J.; Immelman, M.; Lamprecht, G. J.; Greyling, S. E.; Swarts, J. C. *S. Afr. J. Chem.* **1997**, *50*, 208. (d) Klapars, A.; Campos, K. R.; Chen, C.; Volante, R. P. *Org. Lett.* **2005**, *7*, 1185.

(3) (a) Gross, A.; Hüsken, N.; Schur, J.; Raszeja, L.; Ott, I.; Metzler-Nolte, N. *Bioconjugate Chem.* **2012**, *23*, 1764. (b) Shago, R. F.; Swarts, J. C.; Kreft, E.; van Rensburg, C. E. J. *Anticancer Res.* **2007**, *27*, 3431. (c) Maschke, M.; Lieb, M.; Metzler-Nolte, N. *Eur. J. Inorg. Chem.* **2012**, *2012*, 5953. (e) Ott, I.; Kowalski, K.; Gust, R.; Maurer, J.; Mücke, P.; Winter, R. F. *Bioorg. Med. Chem. Lett.* **2010**, *20*, 866.

(4) Spanig, F.; Kovacs, C.; Hauke, F.; Ohkubo, K.; Fukuzumi, F.; Guldi, D. M.; Hirsch, A. *J. Am. Chem. Soc.* **2009**, *131*, 8180.

(5) Pike, A. R.; Ryder, L. C.; Horrocks, B. R.; Clegg, W.; Connolly, B. A.; Houlton, A. *Chem. - Eur. J.* **2005**, *11*, 344.

(6) (a) Chiang, C. C.; Chen, H.-C.; Lee, C.-S.; Leung, M.-K.; Lin, K.-R.; Hsieh, K.-H. *Chem. Mater.* **2008**, *20*, 540. (b) Carter, C.; Brumbach, M.; Donley, C.; Hreha, R. D.; Marder, S. R.; Domercq, B.; Yoo, S.-H.; Kippelen, B.; Armstrong, N. R. *J. Phys. Chem. B* **2006**, *110*, 25191. (c) Özdemir, S.; Balan, A.; Baran, D.; Doğan, O.; Toppare, L. *J. Electroanal. Chem.* **2010**, *648*, 184.

(7) (a) Rosenblum, M. *Chemistry of the iron group metallocenes: ferrocene, ruthenocene, osmocene;* John Wiley & Sons: New York, 1965. (b) Claus, R.; Lewtak, J. P.; Muller, T. J.; Swarts, J. C. *J. Organomet. Chem.* **2013**, *740*, 61. (c) Cook, M. J.; Chambrier, I.; White, G. F.; Fourie, E.; Swarts, J. C. *Dalton Trans.* **2009**, 1136. (d) Stepnicka, P. *Ferrocenes: Ligands, Materials and Biomolecules;* John Wiley & Sons, Ltd: Chichester, U.K, 2008.

(8) (a) Connelly, N. G.; Geiger, W. E. *Chem. Rev.* **1996**, *96*, 877. (b) Hildebrandt, A.; Schaarschmidt, D.; Van As, L.; Swarts, J. C.; Lang, H. *Inorg. Chim. Acta* **2011**, *374*, 112. (c) Pfaff, U.; Hildebrandt, A.; Schaarschmidt, D.; Hahn, T.; Liebing, S.; Kortus, J.; Lang, H. *Organometallics* **2012**, *31*, 6761.

(9) (a) Watts, W. E. In *Comprehensive Organoetallic Chemistry;* Pergamon: Oxford, U.K, 1982; Vol *8*, Chapter 59. (b) Otto, S.; Roodt, A.; Erasmus, J. J. C.; Swarts, J. C. *Polyhedron* **1998**, *17*, 2447 (c).

(10) (a) (a) Mino, T.; Segawa, H.; Yamashita, M. *J. Organomet. Chem.* **2004**, *689*, 2833. (b) Conradie, J.; Lamprecht, G. J.; Roodt, A.; Swarts, J. C. *Polyhedron* **2007**, *26*, 5075. (c) Garabatos-Perera, J.R.; Butenschön, H. *J. Mol. Catal. A: Chem.* **2003**, *196*, 55.

(11) (a) Chantson, J. T.; Falzacappa, M. V. V; Crovella, S.; Metzler-Nolte, N. *J. Organomet. Chem.* **2005**, *690*, 4564. (b) Neuse, E. W.; Kanzawa, F. *Appl. Organomet. Chem.* **1990**, *4*, 19. (c) Blom, N. F.; Neuse, E. W.; Thomas, H. G. *Transition Met. Chem.* **1987**, *12*, 301.

(12) (a) Maitlis, P. M.; Haynes, A.; Sunley, G. J.; Howard, M. J. *J. Chem. Soc., Dalton Trans.* **1996**, 2187. (b) Cavallo, L.; Solà, M. *J. Am. Chem. Soc.* **2001**, *123*, 12294. (c) Haynes, A.; Maitlis, P. M.; Morris, G. E.; Sunley, G. J.; Adams, H.; Badger, P. W.; Bowers, C. M.; Cook, D.

DOI: 10.1021/acs.inorgchem.5b02936
Inorg. Chem. XXXX, XXX, XXX−XXX

B.; Elliott, P. I. P.; Ghaffar, T.; Green, H.; Griffin, T. R.; Payne, M.; Pearson, J. M.; Taylor, M. J.; Vickers, P. W.; Watt, R. J. *J. Am. Chem. Soc.* **2004**, *126*, 2847. (d) Jones, J. *Platinum Met. Rev.* **2000**, *44*, 94.
(13) (a) Andersen, K. K.; Bernstein, D. T. *J. Chem. Educ.* **1978**, *55*, 159. (b) Andersen, K. K.; Bernstien, D. T.; Caret, R. L.; Romanczyk, L. J. *Tetrahedron* **1982**, *38*, 1965. (c) Wood, W. F.; Sollers, B. G.; Dragoo, G. A.; Dragoo, J. W. *J. Chem. Ecol.* **2002**, *28*, 1865.
(14) Hatch, R. C.; Clark, J. D.; Join, A. V. *Am. J. Vet.* **1978**, *39*, 1411.
(15) Sevier, C. S.; Kaiser, C. A. *Nat. Rev. Mol. Cell Biol.* **2002**, *3*, 836.
(16) (a) Badireddy, A. R.; Chellam, S.; Yanina, S.; Gassman, P.; Rosso, K. M. *Biotechnol. Bioeng.* **2008**, *99*, 634. (b) Badireddy, A. R.; Korpol, B. R.; Chellam, S.; Gassman, P. L.; Engelhard, M. H.; Lea, A. S.; Rosso, K. M. *Biomacromolecules* **2008**, *9*, 3079. (c) Vaerewijck, M. J. M.; Huys, G.; Palomino, J. C.; Swings, J.; Portaels, F. *FEMS Microbiology Reviews* **2005**, *29*, 911. (d) Codony, F.; Domenico, P.; Mas, J. *J. Appl. Microbiol.* **2003**, *95*, 288. (e) Baker B. H. J. (Microbion Corporation), US Patent No. US20130224258 A1, Aug 29, 2013.
(17) (a) Chapman, R. G.; Ostuni, E.; Yan, L.; Whitesides, G. M. *Langmuir* **2000**, *16*, 6927. (b) Kim, T.; Crooks, R. M. *Tetrahedron Lett.* **1994**, *35*, 9501. (c) Li, Z.; Lieberman, M.; Hill, W. *Langmuir* **2001**, *17*, 4887. (d) Revell, D. J.; Chambrier, I.; Cook, M. J.; Russell, D. A. *J. Mater. Chem.* **2000**, *10*, 31.
(18) (a) Vogel, A. I. *Practical Organic Chemistry, Including Qualitative Organic Analysis,* 3rd ed.; Longman: London, U.K, 1992; pp 496−501. (b) March, J. *Advanced Organic Chemistry: Reactions, Mechanisms, and Structure,* 4th ed.; John Wiley and Sons: New York, 1992; p 1298.
(19) Kazemekaite, M.; Bulovas, A.; Smirnovas, V.; Niaura, G.; Butkus, E.; Razumas, V. *Tetrahedron Lett.* **2001**, *42*, 7691.
(20) Creager, S. E.; Rowe, G. K. *J. Electroanal. Chem.* **1994**, *370*, 203.
(21) Kondo, T.; Takechi, M.; Sato, Y.; Uosaki, K. *J. Electroanal. Chem.* **1995**, *381*, 203.
(22) (a) Brewster, J. H. *J. Am. Chem. Soc.* **1954**, *76*, 6364. (b) Furniss, B. S.; Hannaford, A. J.; Smith, P. W. G.; Tatchell, A. R. *Vogel's Textbook of Practical Organic Chemistry,* 5th ed.; Longman: New York, 1994; pp 376−378, 519−531.
(23) Cattabriga, M.; Ferri, V.; Tran, E.; Galloni, P.; Rampi, M. A. *Inorg. Chim. Acta* **2007**, *360*, 1095.
(24) Curtin, L. S.; Peck, S. R.; Tender, L. M.; Murray, R. W.; Rowe, G. K.; Creager, S. E. *Anal. Chem.* **1993**, *65*, 386.
(25) Kumar, J.; Purohit, C. S.; Verma, S. *Chem. Commun.* **2008**, 2526−2528.
(26) Marrani, A. G.; Cattaruzza, F.; Decker, F.; Galloni, P.; Zanoni, R. *Electrochim. Acta* **2010**, *55*, 5733.
(27) Müller-Meskamp, L.; Karthäuser, S.; Waser, R.; Homberger, M.; Wang, Y.; Englert, U.; Simon, U. *Surf. Sci.* **2009**, *603*, 716.
(28) Davis, W. L.; Shago, R. F.; Langner, E. H. G.; Swarts, J. C. *Polyhedron* **2005**, *24*, 1611.
(29) Gotzmer, C. US patent 1980, US 4219490 A 19800826.
(30) (a) Mueller-Meskamp, L.; Karthaeuser, S.; Zandvliet, H. J. W.; Homberger, M.; Simon, U.; Waser, R. *Small* **2009**, *5*, 496. (b) Mueller-Meskamp, L.; Karthaeuser, S.; Waser, R.; Homberger, M.; Wang, Y.; Englert, U.; Simon, U. *Surf. Sci.* **2009**, *603*, 716.
(31) (a) Wagner, G.; Herrmann, R. Chiral Ferrocene Derivatives. In *Ferrocenes;* Togni, A. Hayashi, T., Eds.; VCH: Weinheim, Germany, 1995; pp 175−176. (b) Nesmeyanov, A. N.; Kazakova, L. I.; Reshetova, M. D.; Kazitsina, L. A.; Perevalova, E. G. *Bull. Acad. Sci. USSR, Div. Chem. Sci.* **1970**, *19*, 2639−2641.
(32) (a) Hisatome, M.; Yoshihashi, M.; Masuzoe, K.; Yamakawa, K.; Iitaka, Y. *Organometallics* **1987**, *6*, 1498−1502. (b) Niu, H.-T.; Yin, Z.; Su, D.; Niu, D.; Ao, Y.; He, J.; Cheng, J.-P. *Tetrahedron* **2008**, *64*, 6300.
(33) Nishio, T. *J. Chem. Soc., Perkin Trans. 1* **1993**, 1113.
(34) Jesberger, M.; Davis, T. P.; Barner, L. *Synthesis* **2003**, *13*, 1929.
(35) (a) Boguslavskii, L. I.; Sobenina, L. N.; Mikhailik, Yu. V.; Mikhaleva, A. I.; Petrova, O. V.; Es'kova, L. A.; Morozova, L. V.; Skotheim, T. A.; Trofimov, B. A. *Dokl. Akad. Nauk* **1997**, *353*, 51. (b) Misterkiewicz, B.; Dabard, R.; Darchen, A.; Patin, H. *C. R. Acad. Sci., Ser. II* **1989**, *309*, 875. (c) Ratajczak, A.; Czech, B.; Dominiak, M.; Piorko, A. *Polym. J. Chem.* **1980**, *54*, 241.
(36) Song, Q.-B.; Li, Y.-Z.; Liang, Y.-M.; Ma, Y.-X. *Acta Crystallogr., Sect. E: Struct. Rep. Online* **2003**, *59*, m861.
(37) Dinoi, C.; Prikhodchenko, P.; Demirhan, F.; Gun, J.; Lev, O.; Daran, J.-C.; Poli, R. *J. Organomet. Chem.* **2007**, *692*, 2599.
(38) Brader, M. L.; Ainscough, E. W.; Baker, E. N.; Brodie, A. M.; Lewandoski, D. A. *J. Chem. Soc., Dalton Trans.* **1990**, 2089.
(39) Thich, J. A.; Lalancette, R. A.; Potenza, J. A.; Schugar, H. J. *Inorg. Chem.* **1976**, *15*, 2731.
(40) Ren, B.-D.; Zhao, Y.-J. *Acta Crystallogr., Sect. E: Struct. Rep. Online* **2006**, *62*, m170.
(41) Swarts, J. C.; Langner, E. H. G.; Krokeide-Hove, N.; Cook, M. J. *J. Mater. Chem.* **2001**, *11*, 434.
(42) Herberhold, M.; Nuyken, O.; Pohlman, T. *J. Organomet. Chem.* **1995**, *501*, 13.
(43) Gericke, H. J.; Barnard, N. I.; Erasmus, E.; Swarts, J. C.; Cook, M. J.; Aquino, M. A. S. *Inorg. Chim. Acta* **2010**, *363*, 2222.
(44) (a) Evans, D. H.; O'Connell, K. M.; Petersen, R. A.; Kelly, M. J. *J. Chem. Educ.* **1983**, *60*, 290. (b) Kissinger, P. T.; Heineman, W. R. *J. Chem. Educ.* **1983**, *60*, 702. (c) Van Benschoten, J. J.; Lewis, J. Y.; Heineman, W. R.; Roston, D. A.; Kissinger, P. T. *J. Chem. Educ.* **1983**, *60*, 772. (d) Mabbott, G. A. *J. Chem. Educ.* **1983**, *60*, 697.
(45) Bond, A. M.; Oldham, K. B.; Snook, G. A. *Anal. Chem.* **2000**, *72*, 3492.
(46) Eckermann, A. L.; Feld, D. J.; Shaw, J. A.; Meade, T. J. *Coord. Chem. Rev.* **2010**, *254*, 1769.
(47) (a) Bard, A. J.; Faulkner, R. L. *Electrochemical Methods: Fundamentals and Applications,* 2nd ed.; John Wiley & Sons, Inc: New York, 2001. (b) Brown, A. P.; Anson, F. C. *Anal. Chem.* **1977**, *49*, 1589. (c) Laviron, E. *J. Electroanal. Chem. Interfacial Electrochem.* **1979**, *100*, 263.
(48) Laviron, E. *J. Electroanal. Chem. Interfacial Electrochem.* **1979**, *101*, 19.
(49) Weber, K.; Hockett, L.; Creager, S. *J. Phys. Chem. B* **1997**, *101*, 8286.
(50) Hong, H.-G.; Park, W.; Yu, E. *J. Electroanal. Chem.* **1999**, *476*, 177.
(51) Lednicer, D.; Mashburn, T. A., Jr.; Hauser, C. R. *Org. Synth.* **1960**, *40*, 52.
(52) Beagley, P.; Blackie, M. A. L.; Chibale, K.; Clarkson, C.; Moss, J. R.; Smith, P. J. *J. Chem. Soc., Dalton Trans.* **2002**, 4426.
(53) Anne, A.; Blanc, B.; Moiroux, J. *Bioconjugate Chem.* **2001**, *12*, 396.
(54) Lednicer, D.; Lindsay, J. K.; Hauser, C. R. *J. Org. Chem.* **1958**, *23*, 653.
(55) Chatelain, G.; Meyer, A.; Morvan, F.; Vasseur, J.-J.; Chaix, C. *New J. Chem.* **2011**, *35*, 893.
(56) Tran, T. K.; Bricaud, Q.; Ocafrain, M. O.; Blanchard, P.; Roncali, J.; Lenfant, S.; Godey, S.; Vuillaume, D.; Rondeau, D. *Chem. - Eur. J.* **2011**, *17*, 5628.
(57) Bublitz, D. E.; Rinehart, K. L. *Org. React.* **1969**, *17*, 76.
(58) Lindsay, J. K.; Hauser, C. R. *J. Org. Chem.* **1957**, *22*, 355.
(59) *APEX2* including SAINT and SADABS; Bruker AXS Inc: Madison, WI, 2012.
(60) Sheldrick, G. M. *Acta Crystallogr., Sect. A: Found. Crystallogr.* **2008**, *A64*, 112.
(61) Farrugia, L. J. J. *J. Appl. Crystallogr.* **1997**, *30*, 565.
(62) Frisch, M. J.; Trucks, G. W.; Schlegel, H. B.; Scuseria, G. E.; Robb, M. A.; Cheeseman, J. R.; Scalmani, G.; Barone, V.; Mennucci, B.; Petersson, G. A.; Nakatsuji, H.; Caricato, M.; Li, X.; Hratchian, H. P.; Izmaylov, A. F.; Bloino, J.; Zheng, G.; Sonnenberg, J. L.; Hada, M.; Ehara, M.; Toyota, K.; Fukuda, R.; Hasegawa, J.; Ishida, M.; Nakajima, T.; Honda, Y.; Kitao, O.; Nakai, H.; Vreven, T.; Montgomery, J. A., Jr.; Peralta, J. E.; Ogliaro, F.; Bearpark, M.; Heyd, J. J.; Brothers, E.; Kudin, K. N.; Staroverov, V. N.; Kobayashi, R.; Normand, J.; Raghavachari, K.; Rendell, A.; Burant, J. C.; Iyengar, S. S.; Tomasi, J.; Cossi, M.; Rega, N.; Millam, N. J.; Klene, M.; Knox, J. E.; Cross, J. B.; Bakken, V.; Adamo, C.; Jaramillo, J.; Gomperts, R.; Stratmann, R. E.; Yazyev, O.; Austin, A. J.; Cammi, R.; Pomelli, C.; Ochterski, J. W.; Martin, R. L.; Morokuma, K.; Zakrzewski, V. G.; Voth, G. A.; Salvador, P.;

DOI: 10.1021/acs.inorgchem.5b02936
Inorg. Chem. XXXX, XXX, XXX−XXX

Dannenberg, J. J.; Dapprich, S.; Daniels, A. D.; Farkas, Ö.; Foresman, J. B.; Ortiz, J. V.; Cioslowski, J.; Fox, D. J. *Gaussian 09,* Revision B.1; Gaussian, Inc: Wallingford, CT, 2009.

(63) (a) Becke, A. D. *J. Chem. Phys.* **1993**, *98*, 5648. (b) Lee, C.; Yang, W.; Parr, R. G. *Phys. Rev. B: Condens. Matter Mater. Phys.* **1988**, *37*, 785.

(64) Weigend, F.; Ahlrichs, R. *Phys. Chem. Chem. Phys.* **2005**, *7*, 3297.

(65) Recent examples from our laboratories: (a) van der Westhuizen, B.; Swarts, P. J.; Strydom, I.; Liles, D. C.; Fernández, I.; Swarts, J. C.; Bezuidenhout, D. I. *Dalton Trans.* **2013**, *42*, 5367. (b) van der Westhuizen, B.; Swarts, P. J.; van Jaarsveld, L. M.; Liles, D. C.; Siegert, U.; Swarts, J. C.; Fernández, I.; Bezuidenhout, D. I. *Inorg. Chem.* **2013**, *52*, 6674. (c) Bezuidenhout, D. I.; van der Westhuizen, B.; Swarts, P. J.; Chatturgoon, T.; Munro, O. Q.; Fernández, I.; Swarts, J. C. *Chem. - Eur. J.* **2014**, *20*, 4974.

(66) McIver, J. W.; Komornicki, A. K. *J. Am. Chem. Soc.* **1972**, *94*, 2625.

(67) Leading references describing the electrochemical activity and behavior of ferrocene and decamethylferrocene in a multitude of organic solvents are (a) Noviandri, I.; Brown, K. N.; Fleming, D. S.; Gulyas, P. T.; Lay, P. A.; Masters, A. F.; Phillips, L. *J. Phys. Chem. B* **1999**, *103*, 6713. (b) Ruiz, J.; Astruc, D. *C. R. Acad. Sci., Ser. IIc: Chim.* **1998**, *1*, 21. (c) Aranzaes, R. J.; Daniel, M. C.; Astruc, D. *Can. J. Chem.* **2006**, *84*, 288. (d) Fourie, E.; Swarts, J. C.; Chambrier, I.; Cook, M. J. *Dalton Trans.* **2009**, 1145.

DOI: 10.1021/acs.inorgchem.5b02936
Inorg. Chem. XXXX, XXX, XXX−XXX